Structural and Rheological Studies on Highly Cross-Linked Polymeric Systems

A Doctoral Thesis

By
Satoshi Maji

Submitted to the Graduate School of Science, Osaka University

February 2014

Acknowledgements

This thesis is based on the study carried out from 2008 to 2014 in the Department of Macromolecular Science, Graduate School of Science, Osaka University.

First of all, I would like to gratefully and sincerely thank Professor Tadashi Inoue. This thesis would not have been possible without his patient guidance and encouragement throughout my research. He has generously provided me with his deep and thorough knowledge and experience of macromolecular physics study to perform my research. I would like to express my genuine gratitude to Associate Professor Osamu Urakawa for invaluable guidance, encouragement and kind consideration. I really appreciate their instruction and feel honored to be a member of their research group.

I am deeply grateful to present and past president of S. B. Research Co. Ltd., Dr. Hiroyuki Tanaka, Mr. Takao Nakagawa and Mr. Yukio Saeki, for giving opportunity of admission to Osaka University and assignment of macromolecular physics study.

I also want to thank Professor Keiichiro Adachi, my master's thesis advisor, for his insightful comments, suggestions for first rheology study of my carrier. His comments lead encouraging me to complete this thesis.

My special thanks are extended to my colleagues of Sumitomo Bakelite group, all present and past members of Inoue laboratory for their kind cooperation.

Finally, I am deeply indebted to my family for their support, patience, and encouragement during the course of my work.

February 2014

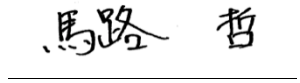

Satoshi Maji

Contents

Chapter 1 General Introduction

1.1. Introduction

Polymeric materials have become indispensable materials for our life today. Industrial progress on 20th century is based on inventions of synthetic polymers including rubbers and plastics and also on developments of processing methods such as molding and forming.

The first industrial use of synthetic polymer was vulcanization of rubbers by Goodyear. This invention is the first example of human control of physical property on naturally occurring polymers. In 1907, Beakeland invented a synthesis process of phenolic resins, which is the first plastic, by only using fossil material. At that time, the phenolic resin was not understood as high molecular weight molecules, and considered as cohering matters of low molecular weight materials. This is because that physical properties of macromolecules were not understood well at that time, and later Staudinger developed macromolecular hypothesis to understand of macromolecule property. Now, the macromolecular hypothesis has been fully accepted, and many polymeric materials were invented after Staudinger's hypothesis. (See Table 1)

Staudinger proposed a viscosity law describing molecular weight dependence of viscosity in solution.

$$\eta_{sp} = K \times M \qquad (1.1)$$

Table 1.1 Chronology of invention of representative synthesized plastics.

Year	Polymer name	Remark
1907	Phenolic resin	Thermosetting
1931	Polyvinyl chloride	Thermoplastic
1938	Polyethylene	Thermoplastic
1939	Polyurethane	Thermoplastic
1940	Polyvinyl alcohol	Thermoplastic
1941	Polyamide (Nylon 6)	Thermoplastic
1943	Epoxy resin	Thermosetting
1949	Polyethylene terephthalate (PET)	Thermoplastic
1957	Polypropylene (PP)	Thermoplastic
1961	Polyimide	Thermoset & plastic
1972	Polyether sulfon (PES)	Thermoplastic
1978	Polyether ether ketone (PEEK)	Thermoplastic

Here, η_{sp}, K and M are specific viscosity, proportional constant and molecular weight, respectively. This law is not strictly correct, but it can give a prediction of the physical properties of high molecular weight molecules. Staudinger's law was empirical formula and there were no model to understand the distinguishing property. Therefore, molecular models of high molecular weight materials are very important to understand physical properties. Today, with the progress of computing technology, the coarse graining model of polymer has become a powerful tool to simulate the properties of macromolecule, for example, elastic constant, viscosity, dielectric constant and so on, for molding process of plastics. Therefore, understanding of the relationship between structure and physical properties, such as mechanical, electrical, thermal properties, is very important. Particularly, molecular dynamics affect to physical properties, and that

of polymers around the glass transition and flow zones are strongly affected by molecular structure, such as branching, cyclic, molecular weight distribution, and cross-linkage pattern. Therefore, the precision understanding of relationship between structure and properties is a fundamental interest in polymer physics even now.

1.2. Structure-Property Relationship of Polymers

Flory showed the athermal conformations of a polymer chain are determined by balance of the effective repulsion energy between monomers and the entropy loss due to stretching by repulsion. In the Flory approximation, the free energy, F, can be written as a sum of the energetic cost F_{int} and the entropic contribution F_{ent}.

$$F = F_{int} + F_{ent} \tag{1.2}$$

For a polymer chain with an excluded volume v, composed of N monomers, each of which are connected with the bond length b, F_{int} and F_{ent} by stretching of chain are estimated by:

$$F_{int} \approx kTv\frac{N^2}{R^3} \tag{1.3}$$

$$F_{ent} \approx kT\frac{R^2}{Nb^2} \tag{1.4}$$

where k is Boltzmann constant, T is absolute temperature and R is the end-to-end

distance of the polymer chain. This Flory theory makes rough estimates of both the energetic and the entropic contribution to the free energy. The energetic cost F_{int} like variation of bond length or bond angle is important for understanding of glass transition, crystallization, compatibility of block copolymer and so on. F_{int} is common to macromolecules, low mass molecules, and metals. For example, Anthony *et al.*[4] showed that the free energy of rubber vulcanizate deformation is mainly depending on the entropic contribution of deformation. Therefore, "polymeric properties" are originated from the entropic contribution. The following paragraphs describe the abstracted molecular models for understanding F_{ent} entropic contribution.

Kuhn showed the freely jointed chain equivalently provides for actual polymers using characteristic length b, is called as Kuhn length.

$$b = \frac{C_\infty N l^2}{R_{max}}. \qquad (1.5)$$

where C_∞, l, and R_{max} is the value at the asymptotic limit at large N for Flory's characteristic ratio, bond length and end-to-end distance of chain, respectively. This picture leads to the coarse graining model of isolated polymer chain having characteristic segment (Kuhn segment).

The molecular dynamics of unentangled linear polymer was successfully modeled by Rouse; the polymer chain is represented as beads connected by springs in the Rouse model.[5] In this model, some monomers compose one bead and spring. This

component is called as viscoelastic segment or Rouse segment. The dynamics of Rouse chain can be calculated by the equation considering the balance of friction of beads, the elastic force by the springs, and the diffusive thermal motion.

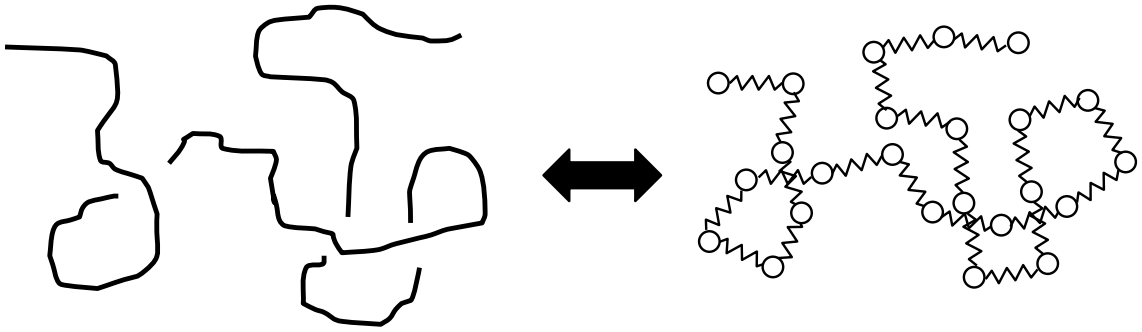

Figure 1.1 The Rouse model, a polymer is coarse graining to N beads connected by +N springs.

The first theory for networks and branching structures was formulated by Flory and Stockmayer in 1940s. Later, the critical percolation theory was successfully applied to gelations in 1970s. Figure 1.2 shows the rough scheme of percolation transition at gelation. These theories have developed a number of growth models to describe the kinetic aspects of aggregation, gelation, and provide, the gel point and the number density distribution of blanching polymer. In addition, dynamics of networks and branching polymers are described by viscoelastic response similarly as liner polymer.

The molecular model of viscoelasticity is required the enough long chain length applying to the coarse graining picture. The ideal polymers are fractal, in case of

ideal linear polymer chain, the fractal dimension, *d*, is 2. Therefore, dynamic scaling rule provides viscoelastic segment has the same property of whole polymer chain. However real polymer chains are not perfectly fractal. Therefore, the scaling rule is limited, if it applies to near segment size region. And for developing the molecular model more and more accurate, the precision analysis of complicated structure near segment size caused by short branch, aggregation of high interaction bond, cross linking and so on, are needed.

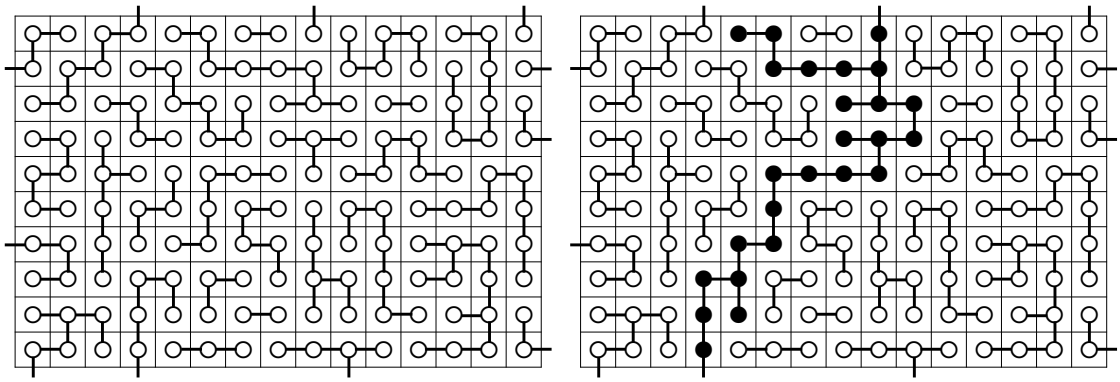

(a)before gelation (b)after gelation

Figure 1.2 A bond percolation transition at gelation. The percolation cluster is indicated by closed circle symbol and bond line.

1.3. Stress Optical Rule and Polymer Dynamics.

The tensile strain, ε, excites polymer chain orientation and birefringence, Δn. The strain-induced birefringence, Δn, is proportional to tensile stress, σ, for polymer melts in relaxation process. This relationship is called the stress-optical rule (SOR). The strain-optical coefficient, O ($=\Delta n/\varepsilon$), is proportional to Young's modulus, E, with a proportional constant, C:

$$\Delta n(t) = C \cdot \sigma(t) \text{ and } O(t) = C \cdot E(t) \quad (1.6)$$

Here, C is called the stress-optical coefficient and t is time, and correlates to the optical anisotropy of segments. The validity of SOR means the molecular origin of both the stress and birefringence is the orientation of segments. In modern theories for viscoelastic properties of polymers, SOR is a fundamental concept to calculate the stress from the chain conformation.

In spite of the SOR is applicable only to polymer melt. Inoue proposed a modified stress-optical rule (MSOR) for the glass transition zone of various polymers.[6] In MSOR, the complex Young's modulus, $E^*(\omega) = E' + iE''$, and the complex stress-optical coefficient in tensile deformation, $O^*(\omega) = O' + iO''$, can be described as the summation of two components, the rubbery and the glassy components (denoted by the subscripts R and G, respectively):

$$E^*(\omega) = E_R^*(\omega) + E_G^*(\omega) \quad (1.7)$$

$$O^*(\omega) = O_R^*(\omega) + O_G^*(\omega) = C_R E_R^*(\omega) + C_G E_G^*(\omega) \quad (1.8)$$

Here, ω is angle frequency. This proposition (the rheo-optical method) made it possible to separate the modulus into the rubbery mode and glassy mode quantitatively. The separation is very useful to discuss the molecular origin of viscoelasticity. For example, the viscoelastic segment size of polymers can be defined from the limiting

modulus of $E_R^*(\omega)$ at high frequencies and the viscoelastic segment size is well correlated with the Kuhn segment size. Today, MSOR are applied to describe the viscoelastic properties of more complex polymeric systems, such as polymacromonomer,[7,8] low-mass molecule/polymer systems,[9,10] block copolymers,[11,12] and so on.

In this study, the rheo-optical method will be extended to highly-blanched polymers and highly crosslinking polymers to clarify their structure-property relationships. The viscoelastic segments or the Kuhn segments for linear polymers are composed of 5-10 repeating units. However, if crosslinking density is extremely increased, the network stand between the crosslinking points can be smaller than these segments. For such a case, the ordinary coarse graining scheme cannot work well. As will be shown later, SOR does not hold valid for highly cross-linked networks. The breakdown of SOR means that we cannot apply the ordinary coarse graining scheme. Consequently, we have to seek a new method to characterize their dynamics.

Hydrogen bonds (H-bonds) also cause crosslinks in the system. The H-bonds are not permanent: they have stronger associating energy (5~30 kJ/mol) than the thermal energy RT~2.5kJ/mol (at room temperature), and therefore they can survive for long time at low temperatures. In the case of polymers, the H-bonding sites are multiple resulting in a complex network structure with long lifetime. In this study, the network structure formed in H-bonding polymer systems will also be discussed.

1.4. Scope of this thesis

By considering above discussion and research background, I intended to study the relationship between the structure and dynamics for highly cross-linked systems by chemical or physical junctions. For this purpose, I examined their dynamic properties by using rheological measurements and their structure by using scattering and spectroscopy methods. The following is the outline of this thesis.

In chapter 2, the relationship between structure and property of novolac resins are analyzed. Novolac resins are very short randomly branched chains. Effects of branched structure on polymer dynamics and viscoelasticity have been studied and consequently well understood, if the chain length is enough long to be applied to the coarse graining picture. However, for the case of very short chains, time scale of chain dynamic is very close to that of the glassy dynamic, and therefore structure-property relationship is not established. More importantly, the coarse graining picture is not a proper method to understand dynamics of very short chains. In this chapter, I clarify the molecular dynamics of branched chains can be well correlated with their structures even for very short chains, if the glassy nature is adequately treated by using GPC, ^{13}C-NMR, DSC and rheo-optical analysis. The obtained chain dynamics apparently follow the scaling rule for long chains.

In chapter 3, relationship of structure and rheological properties of poly (vinyl acetate -co- vinyl alcohol)s, P(VAc-VOH), are discussed. The hydroxyl (OH) group of vinyl alcohol can associate with OH groups themselves or with carbonyl (C=O) groups of vinyl acetate through hydrogen bonds (H-bond). There exist two types of H-bonds

(OH···OH and OH···O=C) and both H-bonds contribute to inter- and intra- chain association. Especially the inter-chain association at multiple points will result in the formation of the quasi branching chain structure, which depends on the OH contents in P(VAc-VOH) copolymers. In this chapter, I describe the H-bonding structure revealed by FT-IR and small angle X-ray scattering (SAXS) measurements. Viscoelastic properties of P(VAc-VOH)s are also described in relation to the aggregation structures and the associated Rouse chain model is used to analyze the data.

In chapter 4, relationship of cross-linking structure and rheological properties of phenolic resins are analyzed. The rubber elasticity theory requires enough length strands for cross-linking structure. Therefore, if network structures have higher crosslinking density than segment size, crosslinking molecular weight M_C do not estimated by rubbery plateau modulus. In this chapter, to clarify the relationship between structure and viscoelastic properties, the dynamic viscoelasticity and dynamic birefringence of phenolic resins were evaluated. In viscoelastic property at low frequency region of high crosslinking phenolic resin, unrelaxed glassy part strongly effect to the modulus. However, birefringence does not affect unrelaxed glassy part so strongly. Therefore, using stress-optical coefficient will provide evaluating of crosslinking pattern of phenolic resins.

Finally, in chapter 5, the obtained results in this thesis are summarized.

1.5. References

1. Flory, P. J., *Principles of Polymer Chemistry*, Cornell University Press: New York,

1953.

2. Rubinstein, M.; Colby, R. H., *Polymer Physics*. Oxford Universiy Press: 2003.
3. Murahashi, S.; Fujita, H.; Kotaka, T.; Kamachi, M., *Polymer Chemistry 4th ed*., Kyoritsu Shuppan: Tokyo, 1993.
4. Anthony, R. L., Caston, R. H., Guth, E. *The Journal of Physical Chemistry*, **1942**, 46, 826-840.
5. Rouse P. E. *The Journal of Chemical Physics*, **1953**, 21, 1272.
6. Inoue, T., Okamoto, H., Osaki, K. *Macromolecules*, **1991**, 24, 5670-5675.
7. Iwawaki, H., Inoue, T., Nakamura, Y. *Macromolecules*, **2011**, 44, 5414-5419.
8. Iwawaki, H., Urakawa, O., Inoue, T., Nakamura, Y. *Macromolecules*, **2012**. 45, 4801-4808.
9. Nobukawa, S., Urakawa, O., Shikata, T., Inoue, T. *Macromolecules*, **2010**, 43, 6099-6105.
10. Nobukawa, S., Urakawa, O., Shikata, T., Inoue, T. *Macromolecules*, **2011**, 44, 8324-8332.
11. Tamura, E., Kawai, Y., Inoue, T., Matsushita, A., Okamoto, S. *Soft Matter*, **2012**. 8, 6161-6166.
12. Tamura, E., Kawai, Y., Inoue, T., Watanabe, H. *Macromolecules*, **2012**. 45, 6580-6586.

Chapter 2 Structure and Viscoelasticity of Novolac Resins

2.1. Introduction

Phenolic resins, which are thermosetting resins, have been attracted attention as promising polymeric materials for their excellent mechanical properties. [1] Phenolic resins are the oldest industrial plastics invented by Beakland in 1907, and have been widely used as insoluble and infusible thermosetting resins in electronics, automotive, housing, and other industries. They are particularly important in automotive application, because light-weight and high-strength plastic materials are desired to design a high fuel-efficient car for a sustainable energy society in near future.

Polymerization involving monomers with their functionality larger than 2, like a phenol resins, leads to the formation of branched polymers and ultimately gels. The problem of polymer gelation has been recognized as a phase transition in connectivity, and percolation ideas have been used to interpret both static and dynamic data.[2-4] There are two universality classes for the gelation problem, distributed by a Ginzburg criterion that depends upon the chain length between branch points, N, [5, 6] as well as the concentration of all nonreacting solvent [7]. In the absence of solvent, the gelation of long linear polymer chains (large N) belongs to the mean-field class and is modeled by Flory-Stockmayer theory [8-10]. The other class is the critical percolation (small N), describes the polymerization of small multifunctional monomers [2, 11, 12].

Novolacs are phenol-formaldehyde resins synthesized in a condition with a formaldehyde to phenol molar ratio of less than one, and are prepolymer of cured phenolic resins. The polymerization is brought to completion using acid-catalysts, such as oxalic acid, hydrochloric acid or sulfonate acids. Novolacs dissolve in organic solvents. Chemical structures of novolacs are shown in Figure 2.1. Methylene groups work as a linker of two phenol units. The linkage of methylene groups can be classified into three types, *o*-*o*′, *o*-*p*′, and *p*-*p*′, depending on three positions that are adjacent to the hydroxyl group of the phenolic ring. Since novolacs are prepolymer of phenolic resins, the same linkage patterns are kept in phenolic resins. It is expected that physical properties of novolacs and phenol resins would depend on the methylene linkage pattern. However, the difference of physical property is not yet clarified in details because the structural analysis of phenolic resins is difficult due to their insolubility and infusibility. In this study, we investigate the effects of linkage pattern on viscoelastic properties of well characterized novolacs to obtain fundamental aspect for mechanical properties of phenolic resins.

Viscoelasticity of randomly branched polymers can be analyzed with dynamic scaling theory based on the Rouse model.[4, 13, 14] The theory is applicable to long chains near the gel point. On the other hand, in case of short chains just after the reaction starts, the glassy nature significantly contributes to the viscoelastic spectra; therefore the interpretation of the viscoelastic property of shot chain is rather complicated. In this study, I analyze the viscoelastic properties of novolacs considering the glassy nature and the randomly branched chain structure. I clarified the structure of threee novolac resins

with different molar mass distributions and methylene linkage patterns. Next, the dynamic moduli of the novolac resins are measured and the viscoelastic spectra were reproduced with the dynamic scaling theory including the glass contribution. We will show that the viscoelastic properties of the novolac resins are well described with the combination of polymeric and glassy modes. Rheo-optical measurement using birefringence measurements make it possible to quantatively separate the modulus into the polymeric mode and the glassy modes.[15] However, the measurements on oligo-polymers were not easy because measurements in shear deformations are necessary, in which the large correction of apparatus compliance is required. Therefore, the molecular dynamics of oligo-polymers were not understood well. We will show that the rheo-optical data can be described consistently with the sum of the polymeric and glassy modes although the frequency range of the data is limited due to large compliance correction.

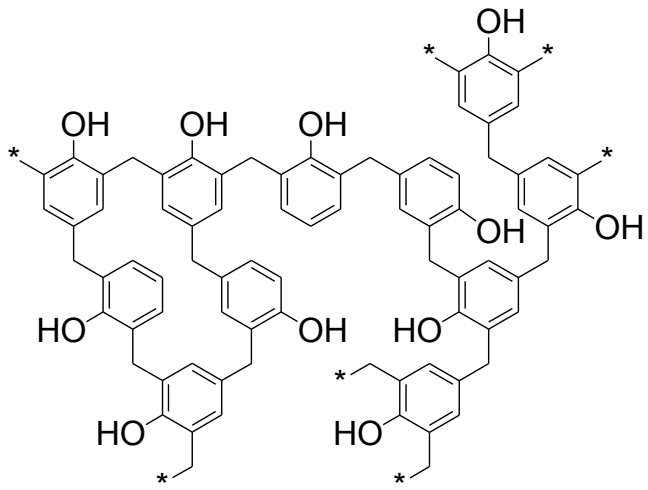

Figure 2.1 Molecular structure of novolacs. Methylene groups connect two phenolic groups.

2.2. Experimental

Typical phenolic resins, random novolac (RN7200) and high ortho novolac (0N1800, ON7800) were supplied from Sumitomo Bakelite Co., LTD. Molar mass and molar mass distribution of novolacs were determined by GPC (Tosoh) and Right Angle Light Scattering (RALS)/Visco detector (TDA302; Viscotek). The bulk density, *d*, of novolacs was estimated to be 1.23 gcm^{-3}.The structures of the novolac resins in methanol solution were characterized by ^{13}C-NMR (ECA-400; JEOL). The glass transition temperature was measured by the modulated differential scanning calorimeter (MDSC 9200; TA Instruments) with the heating and cooling rates were 2 K/min, and modulation rate of ±2 K/min. In the 1st run, temperature was raised from 223K to 473K, and then cooled to 223K. In the 2nd run, the temperature was raised to 473K again. The glass transition temperature was determined by reversing heat flow of the 2nd run.

Complex shear moduli, *G**, of novolacs were measured by ARES rheometer (TA Instruments) with a standard parallel plate fixture of 8mm diameter and a home-made parallel plate fixture 4mm diameter. Instrument compliance was carefully corrected with the method reported by McKenna et al.[16, 17] Composite curves were made for the complex moduli measured in the temperature range from 320 to 430 K, following the method of reduced variables[18].

2.3. Result and Discussion

2.3.1. ^{13}C-NMR

^{13}C-NMR were measured for analyze of the structure of the novolac resins.

Figures 2.2-2.4 show ^{13}C-NMR spectra of the novolac resins. In these spectra, carbons of benzene ring were observed around 158 ppm, and carbons of methylene group were observed around 30-37 ppm. From the intensities of carbons of benzene rings, number fractions of 1) monomer, 2) end (mono-substituted), 3) linear (di-substituted), and 4) branch (tri-substituted) were determined as shown in Figure 2.2. The result is summarized in Table 2.1. ON1800 has higher fraction of end type of phenyl group than ON7800. The branched benzene rings are about 1/3 of the linear units in all samples. he The three novolacs indicate almost the same fraction of branched units. From these values, we estimate that the branching occurs every 4 repeating units in average.

Assuming that no cyclic structure is included, number average molecular weight determined by NMR , M_n^{NMR}, can be calculated from the following equation

$$M_n^{NMR} = \frac{d}{N_{chain}} = \frac{2d}{N_{end} - N_{branch}} \tag{2.1}$$

Here, d is density of novolac. N_{chain}, N_{end} and N_{branch} are the number density of the chain, end and branch, respectively. Since one branching point increases one chain end, ($N_{end} - N_{branch}$)/2 corresponds to N_{chain}. Number average of i-th component, N_i, can be related to the number fraction of i-th component, n_i, determined by NMR measurements.

$$N_i = \frac{d}{M_0} n_i \tag{2.2}$$

Here, M_0 is the molar mass of the repeating unit. The M_n^{NMR} of novolacs are summarized in Table 2.2. M_n^{NMR} of ON1800 and RN 7200 are in accord with the number averaged molecular weight determined by GPC, M_n^{GPC}, however that of ON7800 is not. The reason for this disagreement is not obvious at the present. But I speculate a reason of this disagreement is caused by resolution limitation of GPC column. That is, the molecular weight measurement by light scattering evaluates weight-average molecular weight, therefore the mass distribution of GPC column resolution leads error of number-average molecular weight.

The number of the branching points per chain, ν_B, can be determined from.

$$\nu_B = \frac{N_{branch}}{N_{chain}} \tag{2.3}$$

Here, $\nu_B = 0$ corresponds to linear chains. ν_B of the all novolac samples are approximately 1.5 (Table 2.2), suggesting that they include one or two branching points per chain in average. We note ν_B increases with the increasing of molar mass of the chain. The present small value of ν_B reflects the small chain size of the novolacs. As we have discussed and shown in Table 2.1, the ratio of n_{linear}/n_{branch} is approximately 3, indicating that branching occurs every four phenolic units.

From the value of n_i, we can estimate the extent of the linkage reaction, p.

$$p = \frac{n_{end} + 2n_{linear} + 3n_{branch}}{3} \tag{2.4}$$

The p of the novolacs are summarized in Table 2.2.

From the chemical shift of the methylene groups, the content of each methylene linkage pattern, such as p-p' linkage, were calculated and summarized in Table 2.3. Note that RN7200 has approximately equal contents of the p- and the o-linkage. If we assume that the reaction activity of each o- or p- position of benzene ring is independent of substitution of the other sites, and further assume that the reaction activity the o- site is r times larger than the p- site, then the distribution ratio of various methylene linkage types can be obtained as $4\{r/(2r+1)\}^2$ for o-o' methylene linkage, $4r/(2r+1)^2$ for o-p' linkage, and $\{1/(2r+1)\}^2$ for p-p' linkage. This analysis indicates that reactivity of the o- site is 1.64 times higher than the p- site for ON1800 and ON7800, while reactivity of o- site is half of p- site for RN7200.

We can calculate the n_i values from r and p, and compared them with the experimental data in Table 2.1. They showed good agreement, indicating that the methylene linkage reaction occurred statistically. The critical extent of reaction, p_C, providing $M = \infty$, was estimated to be 0.87-0.89 if we assume the r is constant irrespective of p. At $p = p_c$, the mole fraction of the branched benzene rings is approximately 60%, and the rest is the linear benzene rings. This result indicates that the average monomer number between crosslinking points is approximately one. Note that the present system is far from the gel point, since the p of the present samples are ~0.54.

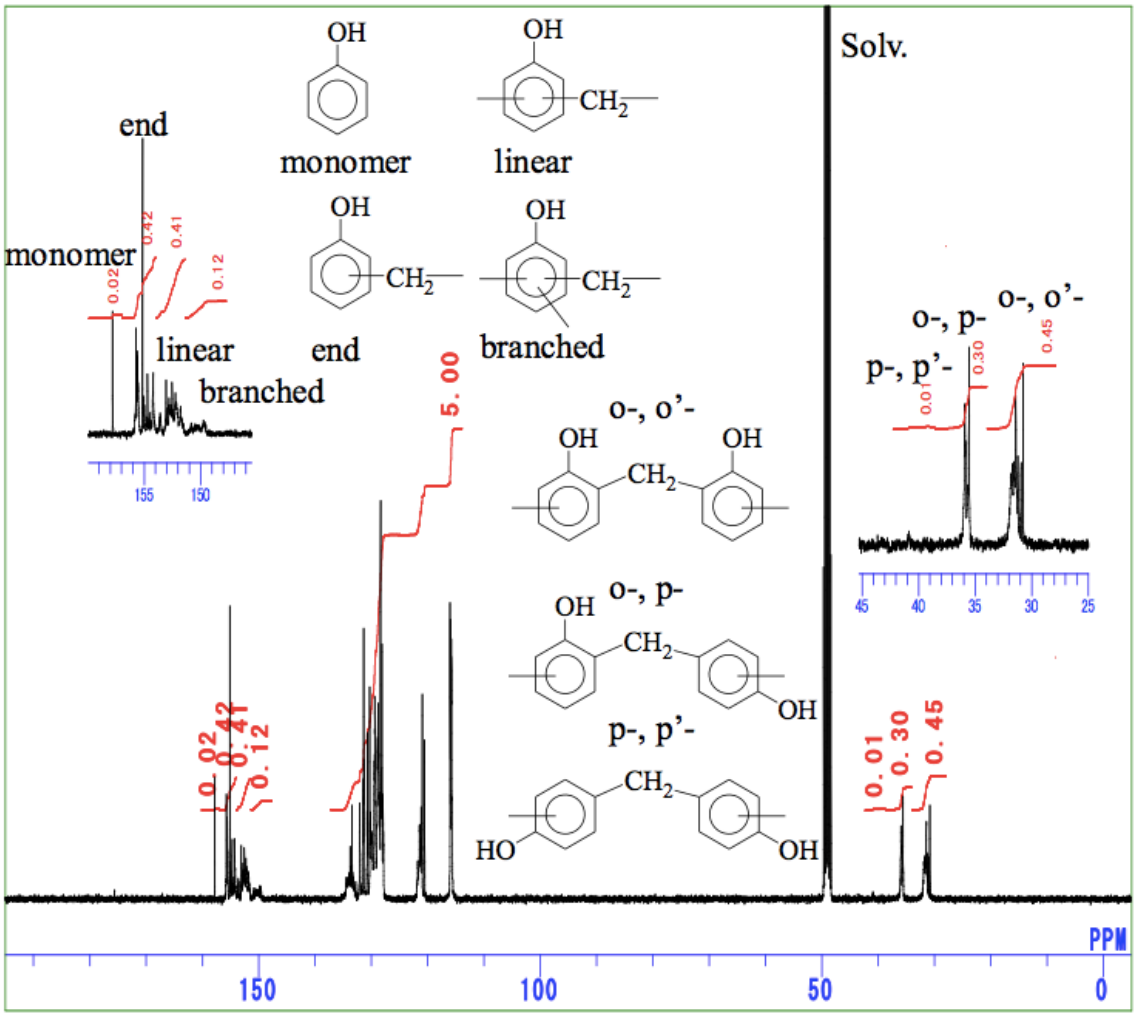

Figure 2.2 ^{13}C-NMR spectra of ON1800.

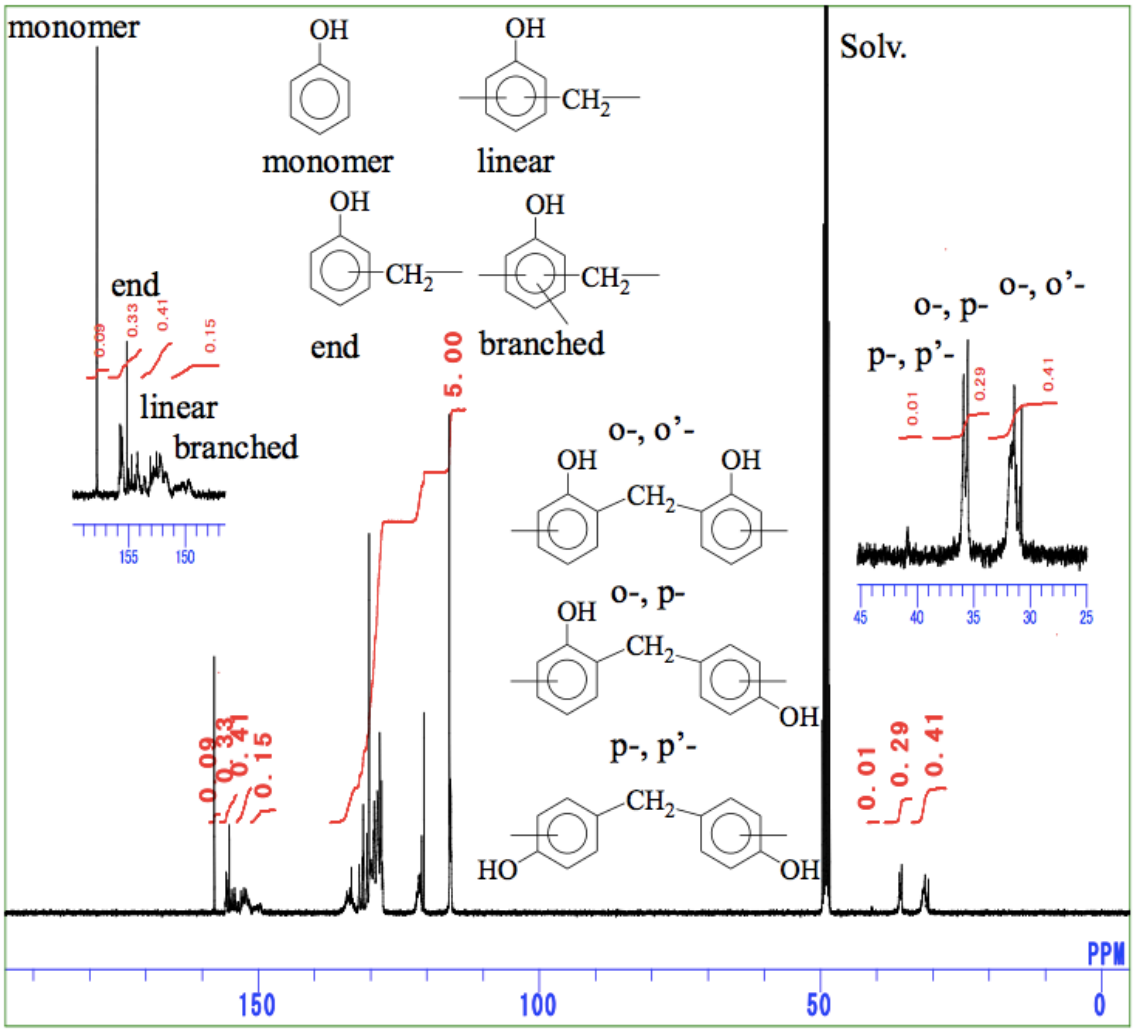

Figure 2.3 ^{13}C-NMR spectra of ON7800

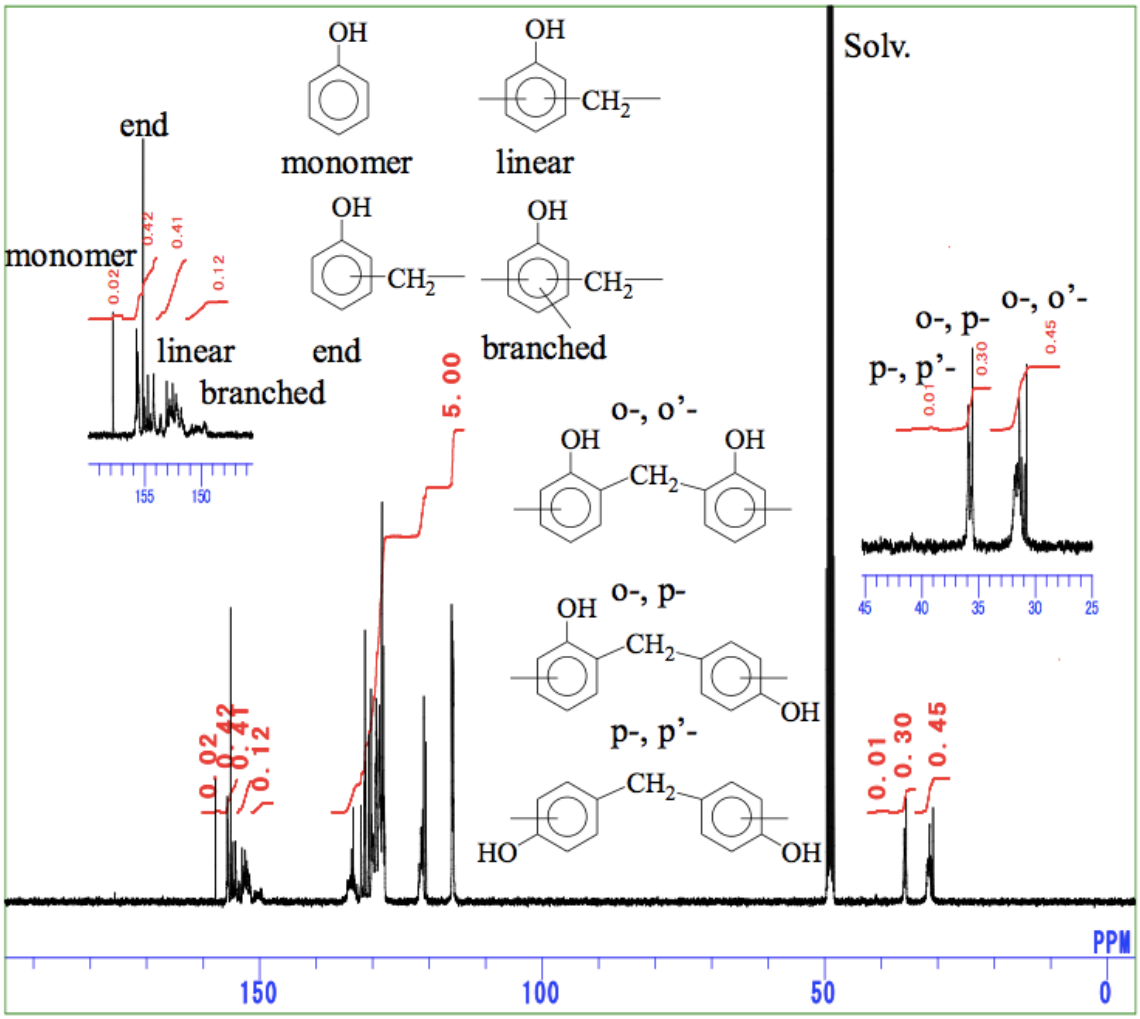

Figure 2.4 ^{13}C-NMR spectra of RN7200

Table 2.1 Characterization of chain end and branching units in the novolacs.

Sample	Experiment				Calculated			
code	monomer	end	linear	branch	monomer	end	linear	branch
ON1800	0.0170	0.442	0.418	0.122	0.0892	0.347	0.418	0.146
ON7800	0.0953	0.333	0.419	0.154	0.0884	0.345	0.419	0.147
RN7200	0.0481	0.385	0.412	0.155	0.0800	0.376	0.412	0.131

Table 2.2 Molar mass, degree of branching, and extent of reaction of the novolacs.

Sample	M_n^{NMR}	M_n^{GPC}	M_w^{GPC}	ν_B	p	p_C
code	$gmol^{-1}$	$gmol^{-1}$	$gmol^{-1}$			
ON1800	663	658	1,800	0.7	0.546	0.8687
ON7800	1140	1660	16,100	1.5	0.541	0.8712
RN7200	922	947	4,410	1.2	0.559	0.8902

Table 2.3 Characterization of methylene linkage types of the novolacs.

Sample	Experiment			calculated			Reactivity	remarks
code	*o*-, *o′*-	*o*-, *p′*-	*p*-, *p*-	*o*-, *o*-	*o*-, *p*-	*p*-, *p*-	ratio of *o*/*p*	
ON1800	0.59	0.39	0.01	0.59	0.36	0.05	1.65	high ortho
ON7800	0.59	0.41	0.00	0.59	0.36	0.05	1.63	high ortho
RN7200	0.27	0.49	0.24	0.25	0.50	0.25	0.50	random

2.3.2. GPC and Intrinsic Viscosity

Molar mass distribution.

Figure 2.5 shows the molecular weight, M, dependence of weight fraction obtained by the GPC measurement. Here, M was determined by light scattering. ON1800 has the lowest molar mass, and ON7800 has significantly broad molar mass distribution. The weight-averaged molecular weight determined by GPC, M_w^{GPC}, and the number-averaged molecular weight determined by GPC, M_n^{GPC}, values are

summarized in Table 2.2. M_n^{GPC} values are consistent with that obtained by NMR, expect for ON7800.

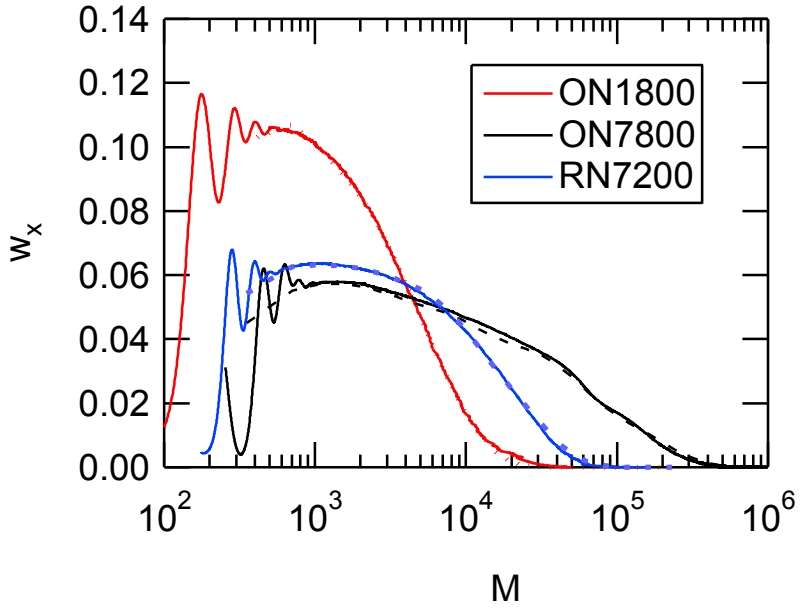

Figure 2.5 Molar mass dependence of weight fraction obtained by the GPC measurement.

The number density of polymers with mass M, $n(M)$, was calculated from eq. 2.5, and shown in Figure 2.6. $n(M)$ obeys a power law for in the low mass region for all the samples, and deviates from the law at a certain molar mass. These features can be captured by the percolation theory, and $n(M)$ was fitted to a power law times a shifted Gaussian cutoff function [19, 20] of the form.

$$n(M) = A\left(\frac{M}{M_{char}}\right)^{-\tau} F\left(\frac{M}{M_{char}}\right) = A\left(\frac{M}{M_{char}}\right)^{-\tau} exp\left[\left\{Z_{max} - \left(\frac{M}{M_{char}}\right)^{\sigma}\right\}^2\right] \qquad (2.5)$$

Here, A is a numerical constant and $F(x)$ is a cutoff function. Numerical simulations showed a maximum in F for a nonzero value of the reduced parameter, Z_{max}, and the numerical data were well described by the above Gaussian curve. [19] The results of fitting to eq. 2.5 are shown in Figure 2.6. The exponents, τ and σ, are summarized in Table 2.4. The exponents, τ and σ, are 2.2 and 0.46, respectively in the critical percolation theory, and 5/2 and 1/2 in the Flory-Stockmayer approach[2, 13], respectively. The experimental results did not agree with these values, but are rather close to τ of hyperbranched polymers: 1.5. Here, hyperbranched polymers means the polymers synthesized from a monomer, AB_{f-1}, that has one functional group (type –A) that differs from the f–1 other ones (type-B). The group A can react with group B, but reaction between two A or between two B groups is impossible. This incisive constraint makes the reaction no longer random. The structure of the hyperbranched polymer from AB_{f-1} is the same as that for the randomly branched polymers from A_f with the f reacting site, but the molar mass distribution is different. [4] Since the experimental result shows $\tau \sim 1$ and $\sigma \sim 0.4$, the novolacs are fairly close to hyperbranched polymers. The agreement with the hyperbranched polymer can be consistently attributed to the fact that the reactivity of *o*- and *p*- sites is not the same. Another reason is that the extent of linkage reaction, p, for our system is far from the percolation threshold, p_c. For the systems far from the percolation threshold or hyperbranched systems from AB_2 type monomers, the number density distribution may be described as follows. [2, 4]

$$n(M) = B\left(\frac{M}{M_{char}}\right)^{-\theta} g\left(\frac{M}{M_{char}}\right) = B\left(\frac{M}{M_{char}}\right)^{-\theta} C^{\left(\frac{M}{M_{char}}\right)} \qquad (2.6)$$

Here, B and C are constants. This scaling rule has been believed to hold valid irrespective of extent of reaction if the system is far from the critical point.[2] The exponent, θ, is determined to be 1 for 2-deimentional systems and θ =1.5 for 3 dimensional systems. [2 4] Deviation from θ =1.5 might be related to the difference in the reactivity of *o*- and *p*- sites.

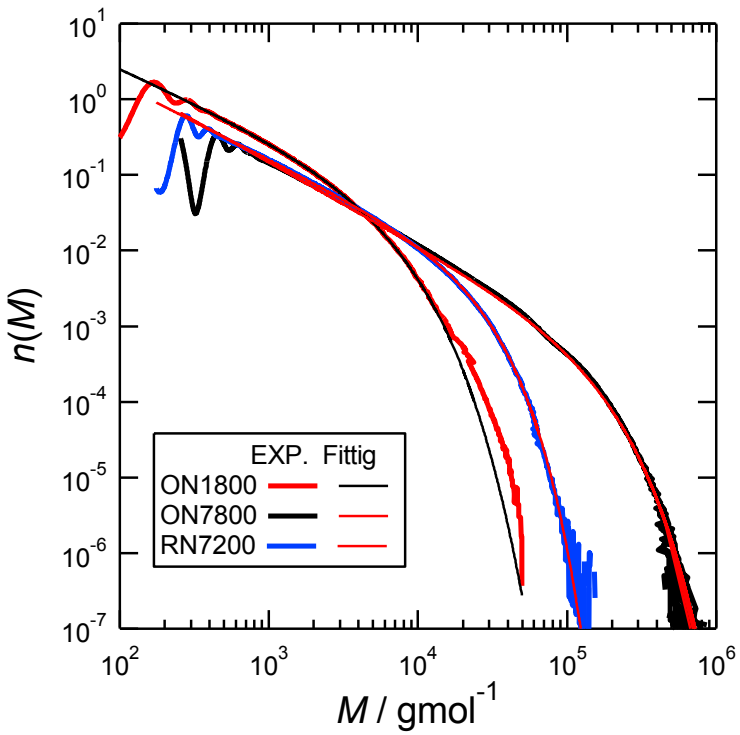

Figure 2.6 GPC data for the novolacs. The curves are two-parameter nonlinear fits to eq. 2.5 using the percolation values for the exponents τ and σ.

An important thing to note is that the average molar mass of the three novolacs is not so high but the molar mass distribution is quite wide for the case of ON7800. In addition, the characteristic molar mass in cutoff function, $M^*{\sim}M_Z$, for ON7800 is over 10^5.

Table 2.4 Static exponents for molar mass distribution.

Sample	τ	σ	M_{char}	θ
ON1800	0.987	0.34	1250	1.0
ON7800	1.20	0.40	40600	1.1
RN7200	1.11	0.46	7900	1.0

Chain dimension.

Figure 2.7 shows the relationship between intrinsic viscosity, [η], and molar mass obtained by the GPC RALS/Visco detector. The figure also included the relationship for the linear polymer, bisphenol A polycarbonate, PC, in THF[21]. The [η] values of novolacs are very close to each other, indicating that the effect of the methylene linkage pattern is small. [η] values of novolacs are smaller than that of PC, indicating that the novolacs have short and compact chain structure.

The theoretical value based on the linear Gaussian chain[22] is represented a purple dashed line in Figure 2.7.

$$[\eta] = \Phi \frac{\langle R^2 \rangle^{\frac{3}{2}}}{M} \tag{2.7}$$

$$\left\langle R^2 \right\rangle = N b_{eff}{}^2 \tag{2.8}$$

Here, Φ is the Flory viscosity coefficient (Φ=2.87×10^{23}), N is the number of bonds per chain, and b_{eff} is the effective bond length. b_{eff} of the freely rotating chain is related to the bond length, b, and bond angle, θ_{i}, at the i-th unit. The novolacs have two bond angles at methylene units and benzene rings, therefore b_{eff} is related to b through the following equation.

$$b_{eff}{}^2 = \frac{1}{2}\left(\frac{1-\cos\theta_1}{1+\cos\theta_1} + \frac{1-\cos\theta_2}{1+\cos\theta_2}\right) b^2 \tag{2.9}$$

The value of b_{eff} is estimated to be 0.74 nm with b=0.294 nm, θ_1=120$^{\mathrm{o}}$, and θ_2=109.5$^{\mathrm{o}}$. The calculated [η] is shown in Figure 2.7. The experimental value of [η] is larger than calculated value at the low M region of M/gmol^{-1}<10^4, while smaller at the high M region.

Addition of the Einstein sphere viscosity, [η]$_{\mathrm{E}}$, provides better agreement at the low M region.

$$[\eta] = \Phi \frac{\left\langle R^2 \right\rangle^{\frac{3}{2}}}{M} + [\eta]_E \tag{2.10}$$

$$[\eta]_E = \frac{2.5}{d} \tag{2.11}$$

Here, d is density. The result based on eq. 2.10 shows better agreement at the low mass region. (Figure 2.7). The. [η] values of novolacs are smaller than those for free rotating chain at high M region, indicating novolacs have a compact chain dimension due to branching.

At high M region, [η] approaches to the power law behavior, $[\eta] \propto M^a$. [13] The exponent, a = 0.44 is very close to a swollen fractal dimension of the randomly branched polymer, a = 0.45, [23] suggesting that the chain dimension of the novolacs is close to a randomly branched chain. Note that the chain dimension of hyperbranched chains agrees well with randomly branched chains. [4] According to eq. 2.10, the exponent, a = 0.44 provides $\langle R^2 \rangle \propto M^{0.96}$ and therefore fractal dimension, D, is 2.08. This value does not agree with 2.53 for fractal dimension of the randomly branched chain. This inconsistency comes from that eq. 2.10 works satisfactorily only for flexible linear chains. The Φ coefficient of branched chains in eq. 2.10 depends on hydrodynamic interactions among the segments,[22] and can be expected to increase slightly with the branching density. The change in the Φ parameter may be taken into account by assuming a power law, $\Phi \sim \Phi_0 M^{0.29}$. [23] And we obtain $D = 3/(a+1-0.29) \sim 2.6$ by this result.

In conclusion, the molar mass distribution did not follow the scaling rule for percolation theory for randomly branched chains. This indicates that the present system does not follow statistically random branching, and rather close to the hyperbranched chains from AB_{f-1} monomers due to the difference of the reactivity of the three site of monomer. Molar mass dependence of [η] also strongly suggests that the chain

dimensions of the novolacs are close to the hyperbranched polymers.

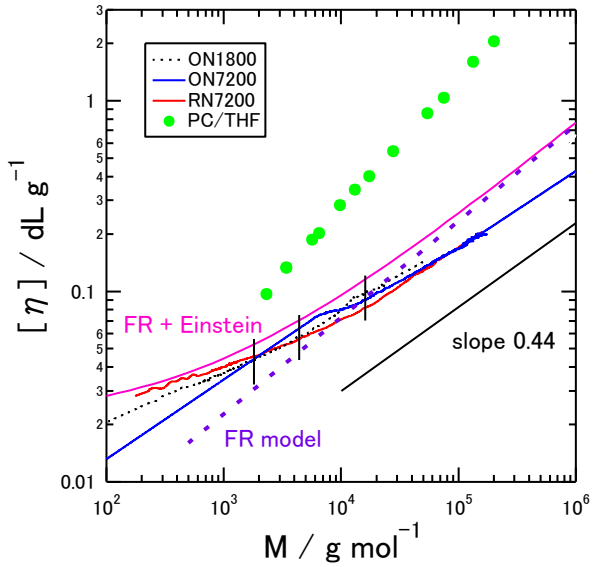

Figure 2.7 Molar mass dependence of intrinsic viscosity for the novolacs in THF. Green circle symbols are intrinsic viscosity of bisphenol A polycarbonate in THF.

2.3.3. Modulated DSC

Figures 2.8 - 2.10 show the results of modulated differential scanning calorimetory (MDSC). Jumps of heat capacities due to the glass transition were observed around 336K, on reversing heat flow of each sample. The glass transition temperature of the 2nd run rises about 20K from the 1st run. This is attributed to the reduction of the residual monomer and the enthalpy relaxation of novolacs. In modulated differential scanning calorimetry, total heat flow is represented by a summation of reversible and nonreversible heat flows.

$$\frac{dH}{dt} = C_P \frac{dT}{dt} + f(T,t) \tag{2.12}$$

Here the first term of the right side represents reversible heat flow, which is configured with heat capacity, melting, and glass transition. The second term of the right side corresponds to nonreversible heat flow, which is configured with chemical reaction, crystallization, evaporation, resolution and enthalpy relaxation. The 1st run of nonreversible heat flow of the novolacs show enthalpy relaxation around 310K and endothermic reaction of polymerization on residual monomer around 340K. In the 2nd run of nonreversible heat flow of the novolacs, enthalpy relaxation and endothermic reaction are not observed, indicating that the novolac resins relax well by heating to 473K.

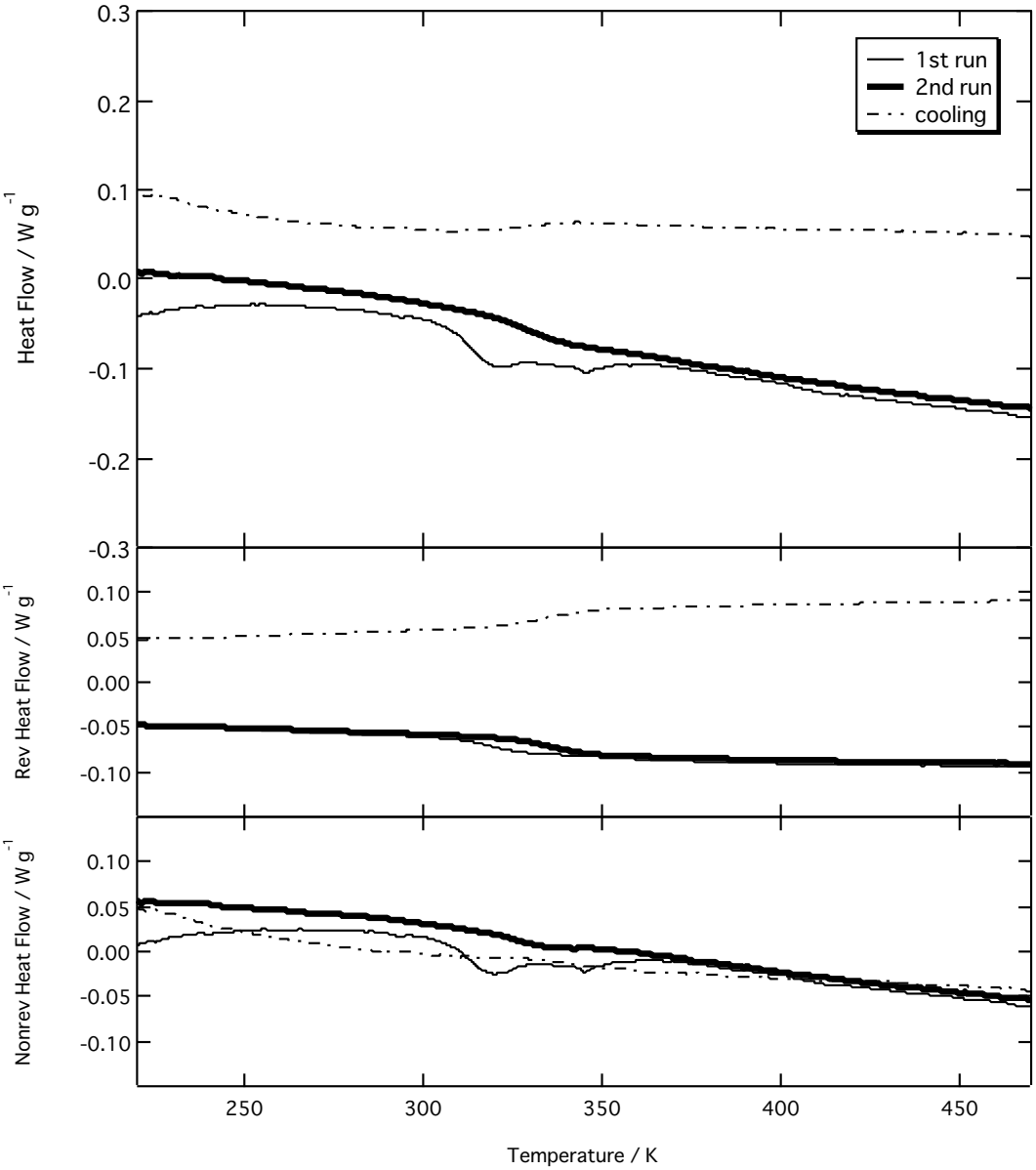

Figure 2.8 Modulated DSC of ON1800.

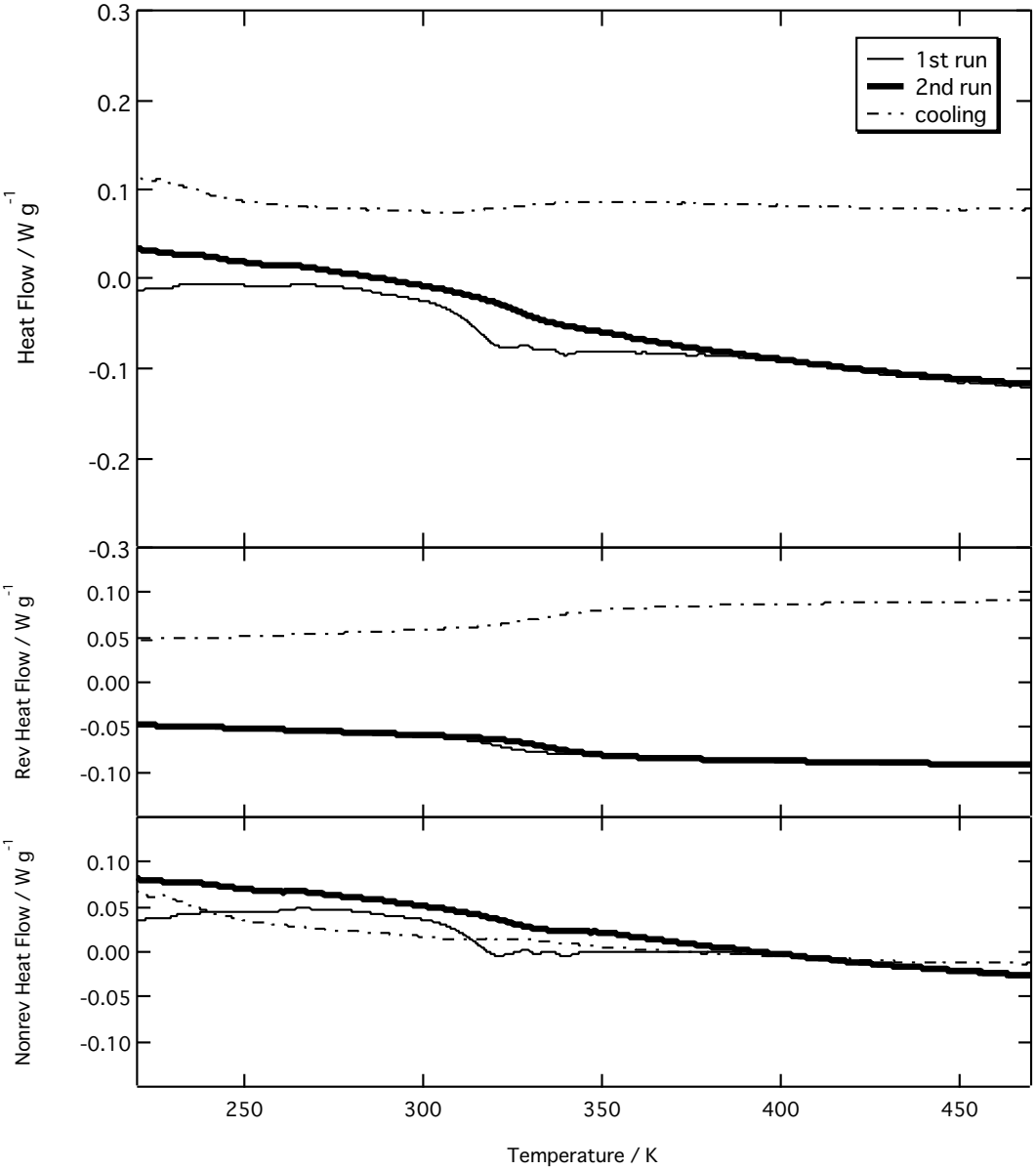

Figure 2.9 Modulated DSC of ON7800.

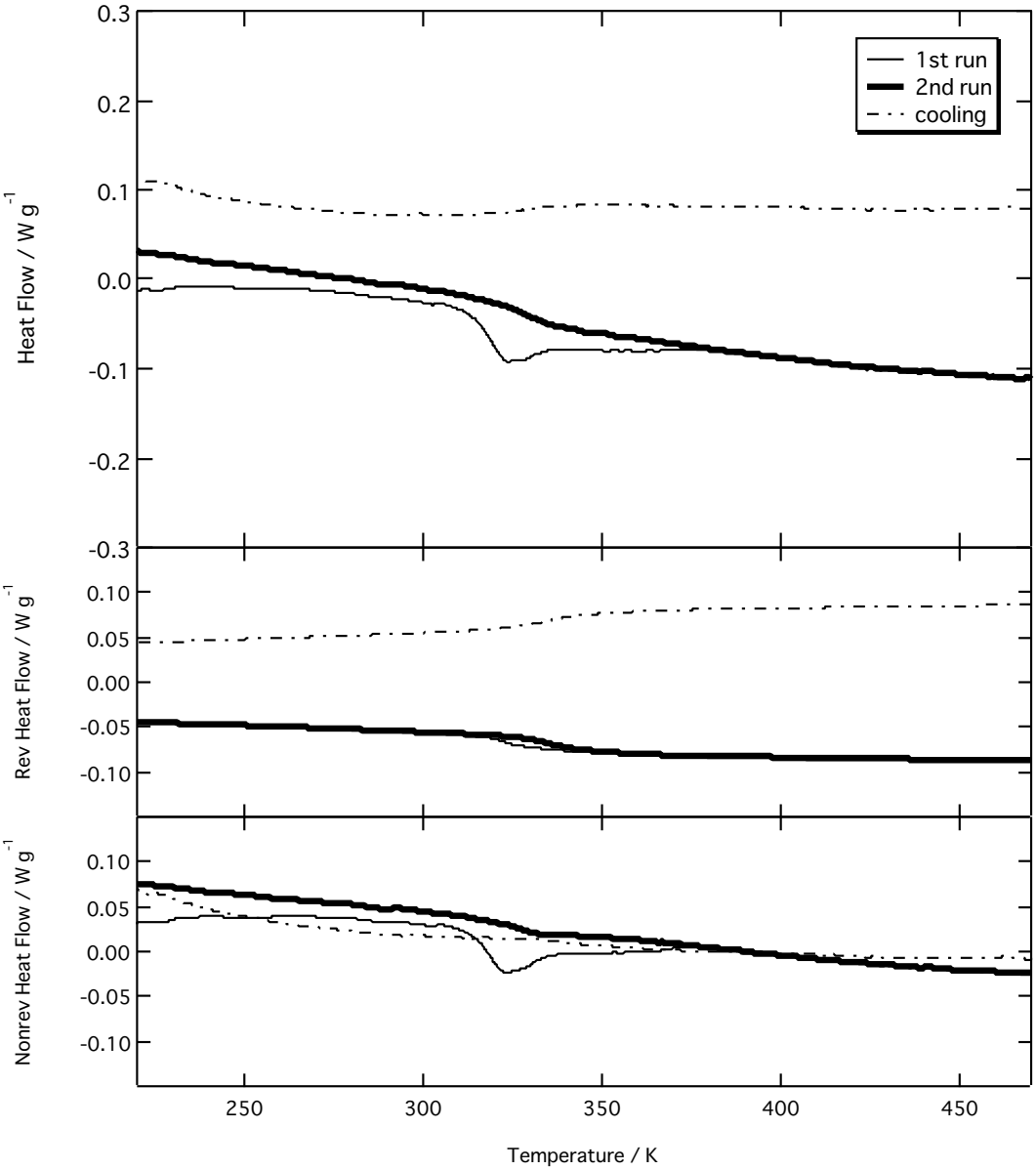

Figure 2.10 Modulated DSC of RN7200.

2.3.4. Complex shear modulus

Overview.

Composite curves of the complex shear moduli, *G**, for the novolac resins are shown in Figure 2.11-2.13. Here, we used the method of reduced variables. [18] In each of *G** curves, in addition to the glassy relaxation around the 10^8Pa range, the additional relaxation mode is observed in *G′* as a shoulder around the 10^5Pa range. These relaxation modes can be assigned to the polymeric modes (the Rouse mode) because molar mass of these samples are about 1000 to 10000. Similar *G** curves are reported for the low molecular weight polystyrenes. [24]

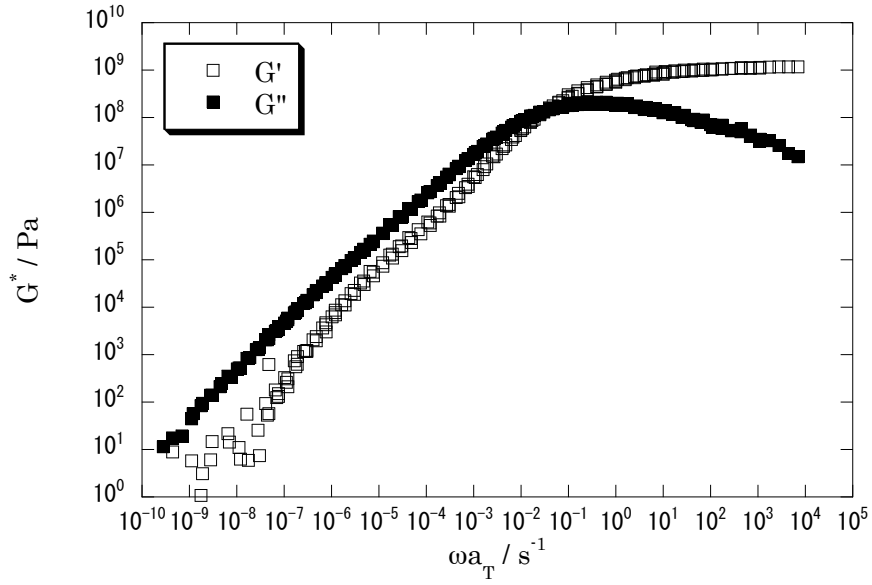

Figure 2.11. Complex shear viscoelasticity of ON7800, reference temperature is 353K.

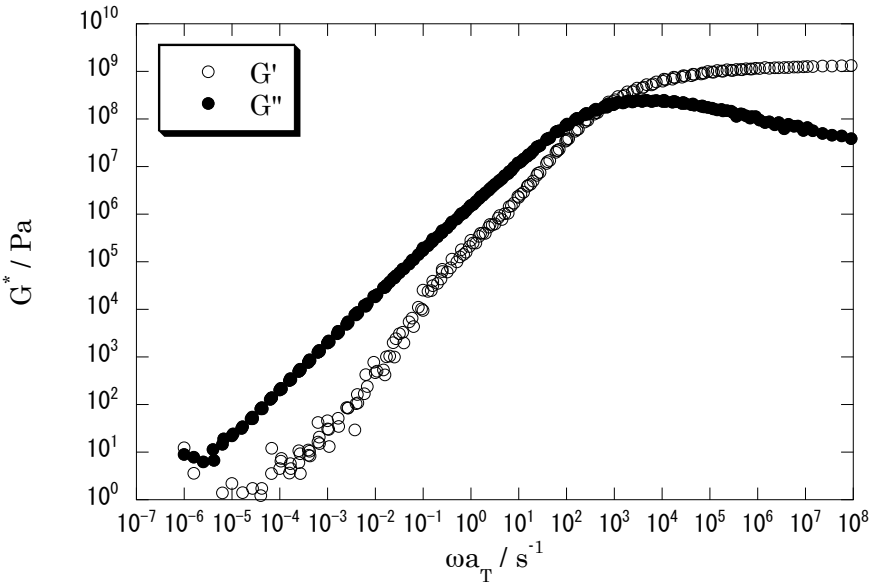

Figure 2.12. Complex shear viscoelasticity of ON1800, reference temperature is 353K.

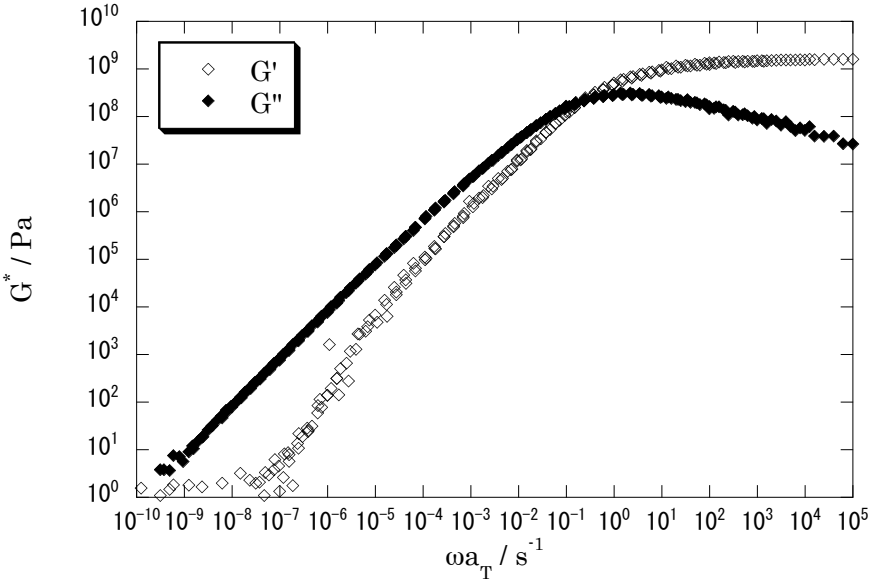

Figure 2.13. Complex shear viscoelasticity of RN7200, reference temperature is 353K.

Temperature dependence.

All the samples have similar viscoelastic spectra and shift factor a_T. The shift factors of all the samples are shown in Figure 2.14. We conclude that the shift factor of

the novolac resins seems to independent of molecular weight and its distribution by comparison of ON1800 and ON7800. And the agreement of ON7800 and RN7200 strongly suggests that shift factor do not depend on type of linkage pattern. The included continuous curve line in Figure 2.14 is calculated by the universal WLF equation.

$$\log a_T = \frac{c_1(T - T_r)}{c_2 + T - T_r} \tag{2.13}$$

Here, c_1 and c_2 is the WLF parameters. If $T_r = T_g + 50$ is chosen, a_T of many polymers follows the universal WLF equation with $c_1 = 8.86$K and $c_2 = 101.6$K. In comparison with WLF equation of shift factor, temperature dependence of a_T of ON7800 and RN 7200 is corresponding with the universal WLF equation well.

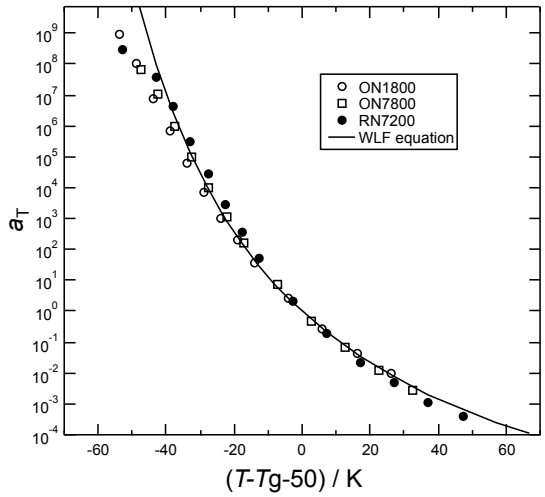

Figure 2.14 Shift factors for novolac resins.

Table 2.5 Glass transition temperature of Novolacs.

Sample code	T_g^{DSC}/K	T_g^{visco}/K
ON1800	327.1	324
ON7800	340.5	344
RN7200	335.9	344

T_g^{visco} is defined as the temperature where the loss modulus shows the maximum at $\omega/s^{-1}= 0.01$.

Comparison of frequency dependence.

Normalized viscoelastic spectra of the three novolac resins are shown in Figure 2.15. Here, the horizontal shift was employed so that each tan δ v.s. ω agrees with each other in the glassy zone for comparison of flow zone. Very small vertical shift was also applied for better superposition. Figure 2.15 indicates that ON7800 has the longest relaxation mode among the three novolacs. This is consistent with that ON 7800 has the longest molecular chain.

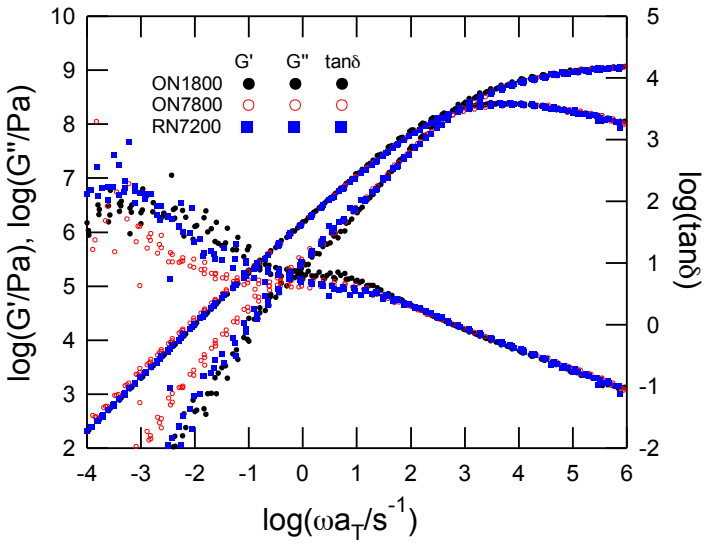

Figure 2.15 Comparison of G^* of the novolac resins.

Figure 2.16 shows a comparison of G^* of ON7800 and the typical glassy response of amorphous polymers. Here we used the G^* data of typical amorphous polymer, polystyrene with M_w=1010,[24] called A1000. The molar mass of the viscoelastic segment size of polystyrene is about 1000 g/mol, and therefore no polymeric mode is observed for G^* of A1000. In the range of $\log(\omega a_T/s^{-1})> 2$, tan δ of the two polymers agrees with each other. At low frequencies, tan δ of A1000 increases quickly with decreasing of ω, indicating that A1000 has a narrower relaxation time distribution than ON7800.

The viscoelastic properties of branched chains have been studied by using dynamical scaling based on the Rouse model. The Rouse time τ_{Rouse} of the polymer chain composed of N beads segment with the length of b,is represented by the following equation. [25]

$$\tau_{Rouse} \approx \frac{\zeta b^3}{k_B T} N^{1+2\nu} \approx \tau_0 N^{1+2\nu} \qquad (2.14)$$

Here, ζ and k_B are friction coefficient of beads and Boltzmann constant, respectively. The parameter, τ_0, is the shortest Rouse relaxation time, and ν is the fractal dimension of the chain. The exponent ν of an ideal linear chain is 1/2. From the dynamic scaling, the polymeric modes (Rouse modes) of the branched chain, G^*_{Rouse}, can be calculated.

As described above, significant contribution of the glassy mode are observed in the viscoelastic spectra of the novolacs. Therefore, G^* of the novolacs were

calculated with the following equation considering the glassy modes, and used for the more detailed discussion.

$$G^*(\omega) = G^*_{\text{Rouse}}(\omega) + G^*_{\text{A1000}}(\omega) \tag{2.15}$$

$$G^*_{\text{Rouse}} = \sum_i w(M_i)\frac{\rho RT}{M_i} G^*_i(\omega) \tag{2.16}$$

$$G^*_i(\omega) = \sum_{p=1}^{N_i} \frac{\omega^2 \tau_{i,p}{}^2 + i\omega\tau_{i,p}}{1 + \omega^2 \tau_{i,p}{}^2} \tag{2.17}$$

$$\tau_{i,p} = \tau_0 \left(\frac{N_i}{p}\right)^{(1/\nu+2)/3} \tag{2.18}$$

In calculation of $G^*_{\text{Rouse}}(\omega)$, we assumed the ordinary linear chains of novolac, $\tau_{i,p} = \tau_0(N_i/p)^2$ to see the effect of branching. The Rouse segment size, M_S, was assumed as 300 g mol^{-1}. The results are shown in Figure 2.16. The value of τ_{Rouse} was chosen so that the calculated G^* agrees with the experimental data at low frequencies. Consequently, the agreement is well at low frequencies. However, in the middle frequency region, $-1 < \log(\omega a_T/\text{s}^{-1}) < 2$, the agreement in G' is not so good. We should note that the shortest Rouse relaxation time, τ_S, is very close to the relaxation time of the glassy component, τ_G. The previous study on the ordinary polymers shows $\tau_S / \tau_G \sim 10$. [26] Thus, we conclude that G_{Rouse}^* of the novolacs should have a narrow relaxation time distribution due to the branching. This is quite natural because branching of chain would causes degeneracy of the longest relaxation mode.

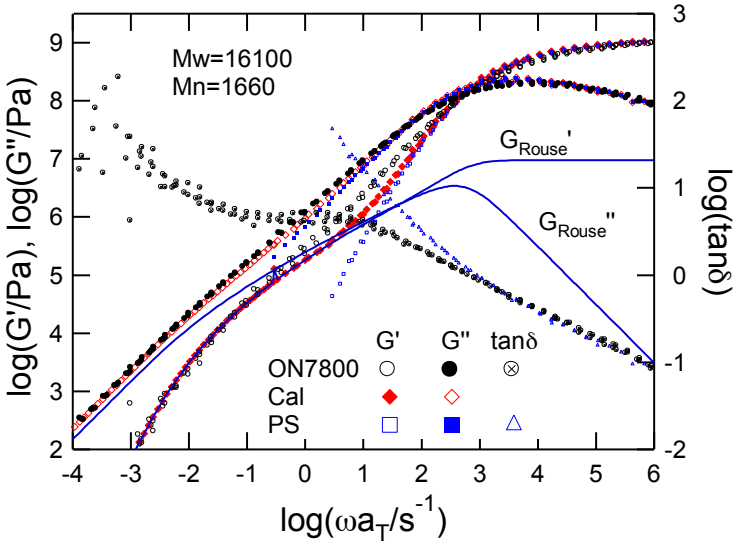

Figure 2.16. Comparison of G^* of ON7800 and glassy modulus (polystyrene, M_w=1000).

As we have discussed before, the molar mass dependence of $[\eta]$ suggests that the novolacs have a similar branching structure with the hyperbranched chains. Since the structure of the hyperbranched chains is identical to the randomly branched chains, we recalculated G_{Rouse}^* of Figure 2.16 with ν =1/2.53 for the randomly branched chain. The result is shown in Figure 2.17. The calculated G^* shows a good agreement with the experimental G^* of ON7800 over the whole frequency region. Thus, viscoelastic analysis indicates that the novolacs can be regarded as a randomly branched chain. This is consistent with the result obtained by the NMR and the intrinsic viscosity measurements.

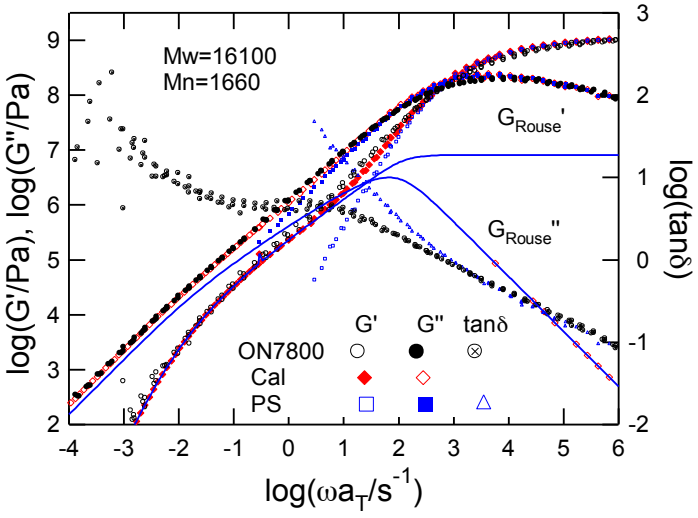

Figure 2.17. Comparison of G^* between experimental data of ON7800 and theoretical calculation with v =1/2.53.

Rheo-optical data.

To clarify the Rouse dynamics of the novolacs more clearly, the dynamic birefringence measurements were conducted.[15] The merit of the rheo-optical method is the quantitative separation of modulus in the component functions, depending on the molecular origin of stress with the modified stress optical rule, MSOR.[15] The method has been utilized for various systems. [27-30] For amorphous polymers, the complex modulus and complex strain-optical coefficient, $K^*(\omega)$, can be separated into the glassy, G^*_G, and the polymeric (rubber) components, $G^*_R(\omega)$.

$$G^*(\omega) = G^*_R(\omega) + G^*_G(\omega) \tag{2.19}$$

$$K^*(\omega) = C_R\, G^*_R(\omega) + C_G\, G^*_G(\omega) \tag{2.20}$$

Here, C_R and C_G are the stress-optical coefficient for the R and G components, respectively. We can determine G^*_R and G^*_G from eqs (2.19) and (2.20). The separation of G^*_R and G^*_G is essentially identical with eq. (2.15). Figure 2.18 shows a preliminary result of G^*_R and G^*_G for RN7200. The applicability of actual measurements in shear deformation is limited near the glass transition because the large compliance correction of apparatus is necessary. As we have predicted, the glassy component, G^*_G, agrees well with G^* of A1000 (low mass polystyrene), indicating that the glassy component of the novolacs is identical to the typical glassy component of amorphous polymers. On the other hand, the polymeric component, G^*_R, is fitted to the Rouse model by eq, (2.16). Here, we used M_S= 350. The curves in the figure shows the results of $(2+1/\nu)/3=1.5$ and 2. Again, $(2+1/\nu)/3=1.5$ gives a better fitting result, supporting the conclusion of the previous section.

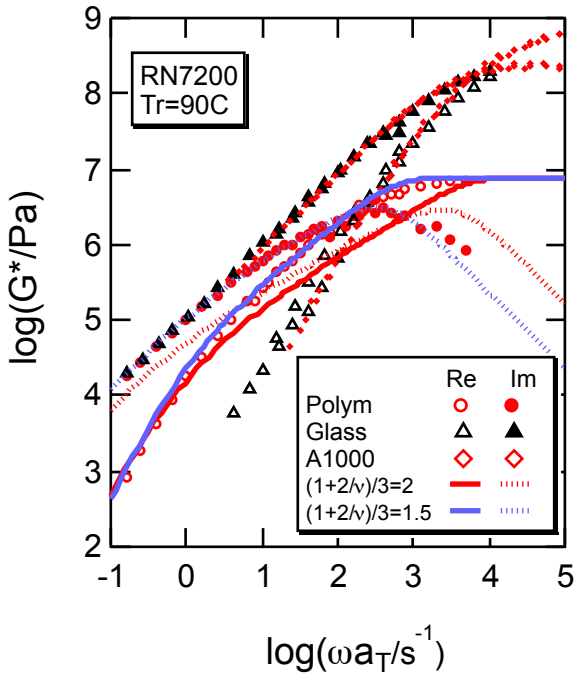

Figure 2.18. Component functions of RN7200. Curves represent calculated complex modulus with the Rouse model.

2.4. Conclusion

We have conducted NMR, GPC, DSC and rheological measurements on three samples to elucidate the relationship between structure and rheological properties of novolacs. Molar mass dependence of the number density did not follow the percolation theory for the randomly branched chains and close to that for hyperbranched chain structure. Molar mass dependence of intrinsic viscosity indicated that the novolacs had a hyperbranched chain structure. This comes from that the extent of reaction of the system is far from the percolation threshold in addition to the different reactivity of three sites of benzene ring. Dynamic moduli of the three novolacs were similar particularly in the glassy zone. Difference of G^* by molar mass is observed at low frequencies. The dynamic modulus originated by chain connectivity (polymeric modes)

was estimated by subtracting the glassy modulus from the shear modulus and was well described by the dynamic scaling theory based on the Rouse model. The exponent for the polymeric modes was found to be ~2/3, which agreed with the dynamic scaling for the randomly branched chains (the same as for the hyperbranched polymers). The methylene linkage pattern of *o-o′*, *o-p′*, and *p-p′* at phenolic rings did not significantly affect the scaling of chain dimension and dynamic modulus.

2.5. References

1. Gardziella, A.; Pilato, L. A.; Knop, A., *Phenolic Resins: Chemistry, Applications, Standardization, Safety and Ecology,*. 2nd completely rev. edn ed.; Springer: Berlin, 1999.
2. Stauffer, D.; Aharony, A., *Introduction to Percolation Theory*. Taylor and Francis: London, 1992.
3. de Gennes, P. G. *Recherche* **1976,** 72, 919.
4. Rubinstein, M.; Colby, R. H., Polymer Physics. In *Polymer Physics*, Oxford Universiyt Press: 2003; p 320.
5. V. L. Ginzburg. *Sov. Phys. Solid State 2, 1824(1960)* **1960,** 2, 2031.
6. de Gennes, P. G. *J. Phys. (France) Lett.* **1977,** 38, L355.
7. Daoud, M. *J. Phys. (France) Lett.* **1979,** 40, L201.
8. Flory, P. J. *J. Am. Chem. Soc.* **1941,** 63, 3083.
9. Stockmayer, W. H. *J. Chem. Phys.* **1943,** 11, 45.
10. Stockmayer, W. H. *J. Chem. Phys.* **1944,** 12, 125.

11. Stauffer, D.; Coniglio, A.; Adam, M. *Adv. Polym. Sci.* **1983,** 44, 103.

12. de Gennes, P.-G., *Scaling Concepts in Polymer Physics*. Cornell University Press: Ithaca: NY, 1979.

13. Lusignan, C. P.; Mourey, T. H.; Wilson, J. C.; Colby, R. H. *Phys Rev E* **1995,** 52, 6271.

14. Lusignan, C. P.; Mourey, T. H.; Wilson, J. C.; Colby, R. H. *Phys Rev E* **1999,** 60, 5657.

15. Inoue, T.; Okamoto, H.; Osaki, K. *Macromolecules* **1991,** 24, 5670.

16. Schroter, K.; Hutcheson, S. A.; Shi, X.; Mandanici, A.; McKenna, G. B. *J Chem Phys* **2006,** 125, 214507.

17. Hutcheson, S. A.; McKenna, G. B. *J Chem Phys* **2008,** 129, 074502.

18. Ferry, J. D., Chapter 11 Dependence of Viscoelastic Behavior on Temperature and Pressure. In *Viscoelastic Properties of Polymers*, 4th *Ed*. ed.; Wiley: New York, 1980; pp 264.

19. Schosseler, F.; Benoit, H.; Grubisic-Gallot, Z.; Strazielle, C.; Leibler, L. *Macromolecules* **1989,** 22, 400.

20. Ottavi, H. *J. Phys. A* **1987,** 20, 1015.

21. Maeda, N.; Norisuye, T. *Polymer* **1993,** 34, 3475.

22. Yamakawa, H., *Modern Theroy of Polymer Solutions*. 1971.

23. Weissmüller, M.; Burchard, W. *Acta Polym* **1997,** 48, 571.

24. Inoue, T.; Onogi, T.; Osaki, K. *J. Polym. Sci. Polym. Phys. Ed.* **1999,** 37, 389.

25. Rubinstein, M.; Colby, R. H.; Gillmor, J. R., In *Space-TIme Organization in*

Macromolecular Fluids, Tanaka, F.; Doi, M.; Ohta, T., Eds. Springer: New York, 1989; p 207.

26. Inoue, T.; Osaki, K. *Macromolecules* **1996,** 29, 1595.
27. Tamura, E.; Kawai, Y.; Inoue, T.; Matsushita, A.; Okamoto, S. *Soft Matter* **2012,** 8, 6161.
28. Tamura, E.; Kawai, Y.; Inoue, T.; Watanabe, H. *Macromolecules* **2012,** 45, 6580.
29. Inoue, T.; Matsumoto, A.; Nakamura, K. *Macromolecules* **2013,** 46, 6104.
30. Maeda, A.; Inoue, T.; Sato, T. *Macromolecules* **2013,** 46, 7118.

Chapter 3 Scattering and Rheological Analysis of Poly (vinyl acetate -co- vinyl alcohol)

3.1. Introduction

Hydrogen (H-) bonding interaction plays an important role in polymer materials for the structure formation, such as crystallization, phase separation, inter- and intra-molecular association, as well as for the molecular dynamics. Properties of a polymer material, e.g., heat resistance, gas barrier properties, solvent resistance, etc., are related to both the molecular interactions, such as hydrogen bonds, and the structures formed in the materials. The relationship between the interaction, structure, and the property should be clarified toward the control of material properties. However, it is not generally known how many interactions of H-bond affect the higher order structures and the properties in polymer materials.

In this study I examined a model system of H-bonding polymer melts in order to clarify the relationship between the number of H-bonds and the resulting aggregated structures. Specifically, random copolymers of vinyl acetate and vinyl alcohol, P(VAc-VOH), with various vinyl alcohol contents (f_{OH}), were used, in which hydrogen bonds between the OH groups and between C=O and the OH groups exist. Aggregation structures characteristic to the H-bonding polymers have been studied via FT-IR, wide-, and small-angle X-ray scattering experiments.

3.2. Experimental

Poly(vinyl acetate) (PVAc) with molecular weight (M_w) 12,000 and 130,000 were purchased from Aldrich Chemicals and used as base polymers to synthesize random copolymers of vinyl acetate (VAc) and vinyl alcohol (VOH) with various VOH contents. Specifically, the copolymers, P(VAc-VOH)s, were obtained through the saponification reaction of the PVAc: adding appropriate amount of NaOH aqueous solution into the PVAc / methanol solution at room temperature[1]. The degree of saponification f_{OH} was controlled by the reaction time and the NaOH concentration, and determined by eq. (3.1) with the ^{1}H-NMR data.

$$f_{OH} = \frac{I_{OH}}{I_{Ac}} \times 100 \quad (3.1)$$

Here, l_{OH} and l_{Ac} are molar fraction of VOH and VAc, respectively. The randomness of sequence distribution, η, of VAc and VOH defined by eq.3.2 was also determined with ^{1}H-NMR.

$$\eta = \frac{(VOH,VAc)}{2f_{OH}(100-f_{OH})} \times 100 \quad (3.2)$$

Here, (VOH, VAc) is a molar fraction of the neighbor unit of VOH and VAc. The continuation of VOH and VAc monomer (mean run number), l_{VOH} and l_{VAc}, are calculated by eqs.3.3 and 3.4.

$$l_{VOH} = \frac{2(VOH)}{(VOH,VAc)} \quad (3.3)$$

$$l_{VAc} = \frac{2(VAc)}{(VOH,VAc)} \quad (3.4)$$

Here, (VOH) and (VAc) is a molar fraction of VOH and VAc, respectively. Table 3.1 shows the characteristics of the samples used in this study.

FT-IR measurements were conducted with the IR spectrometer (EXCALIBUR FTS-3000, DISILAB JAPAN) in the light transmission method on the molten P(VAc-VOH) samples sandwiched between two CaF_2 plates.

Table 3.1 Characteristics of PVAc and P(VAc-VOH)s.

					Mean run number	
Code	10^{-3}Mw	f_{OH}/%	T_g^{DSC}/K	η	l_{VOH}	l_{VAc}
PVAc-12k	12.1	2.0	308	-	-	-
PVAc-130k	130	-	308	-	-	-
P(VAc-VOH10)	(11.6)[a]	10.1	309	0.81	1.37	12.2
P(VAc-VOH18)	(11.2)[a]	18.0	311	0.79	1.55	7.07
P(VAc-VOH28)	(10.6)[a]	27.8	313	0.58	2.39	6.20
P(VAc-VOH34)	(10.2)[a]	34.4	317	0.53	2.86	5.44
P(VAc-VOH37)	(10.1)[a]	37.1	318			
P(VAc-VOH60)	(8.7)[a]	60.4	323	0.50	5.04	3.29
P(VAc-VOH75)	(7.9)[a]	74.5	332	0.50	7.80	2.67
P(VAc-VOH26)-130k	(116)[a]	25.8	315	0.67	2.04	5.74
P(VAc-VOH34)-130k	(110)[a]	35.4	318	0.63	2.47	4.44

[a] Calculated from f_{OH} values.

Wide- and small-angle X-ray scattering (WAXS, and SAXS) measurements were performed to examine the structures formed in bulk P(VAc-VOH)s at BL03XU and BL08B2 in SPring-8 (Japan Synchrotron Radiation Research Institute). The WAXS data were collected on an imaging plate (Fujifilm) with the camera lengths 10 cm, and the SAXS data collected on an imaging plate detector of R-AXIS (RIGAKU) or the PILATUS 1K (Dectris) pixel detector with camera lengths 4.1 m or 6.2 m.

3.3. Result and Discussion

3.3.1. H-Bonding Structures Revealed by FT-IR

Figure 2 shows the FT-IR absorbance spectra for (a) C=O stretching band (1770 – 1680cm^{-1}) and (b) OH stretching band (3660 – 3040cm^{-1}) measured at 40°C. With the increase of the OH content, f_{OH}, the H-bonded C=O observed at around 1716 cm^{-1} as a shoulder of the main peak (free C=O) increases. These spectra were separated into two peaks corresponding to the free and H-bonded C=O, and the molar ratio of these components were determined following the procedure described in Ref.10.

We found that free (non-H-bonded) OH did not exist in bulk. The free OH peak was confirmed to appear at around 3660 cm^{-1} for toluene solution of P(VAc-VOH10). These data suggest that all the OH groups H-bond with C=O or other OH groups. In addition, the peaks of OH stretching band broaden toward lower wave numbers with increasing f_{OH}. This suggests the formation of the linearly H-bonded OH multimer (OH···OH···OH···) and the number of the multiple H-bonds increase.

From the molar content values of C=O groups, which are free or H-bonded with OH

groups, we determined the fraction of the OH groups which are H-bonded with C=O or other OH groups. The result is shown in Figure 3.3, indicating that the main H-bonded species is OH···OH.

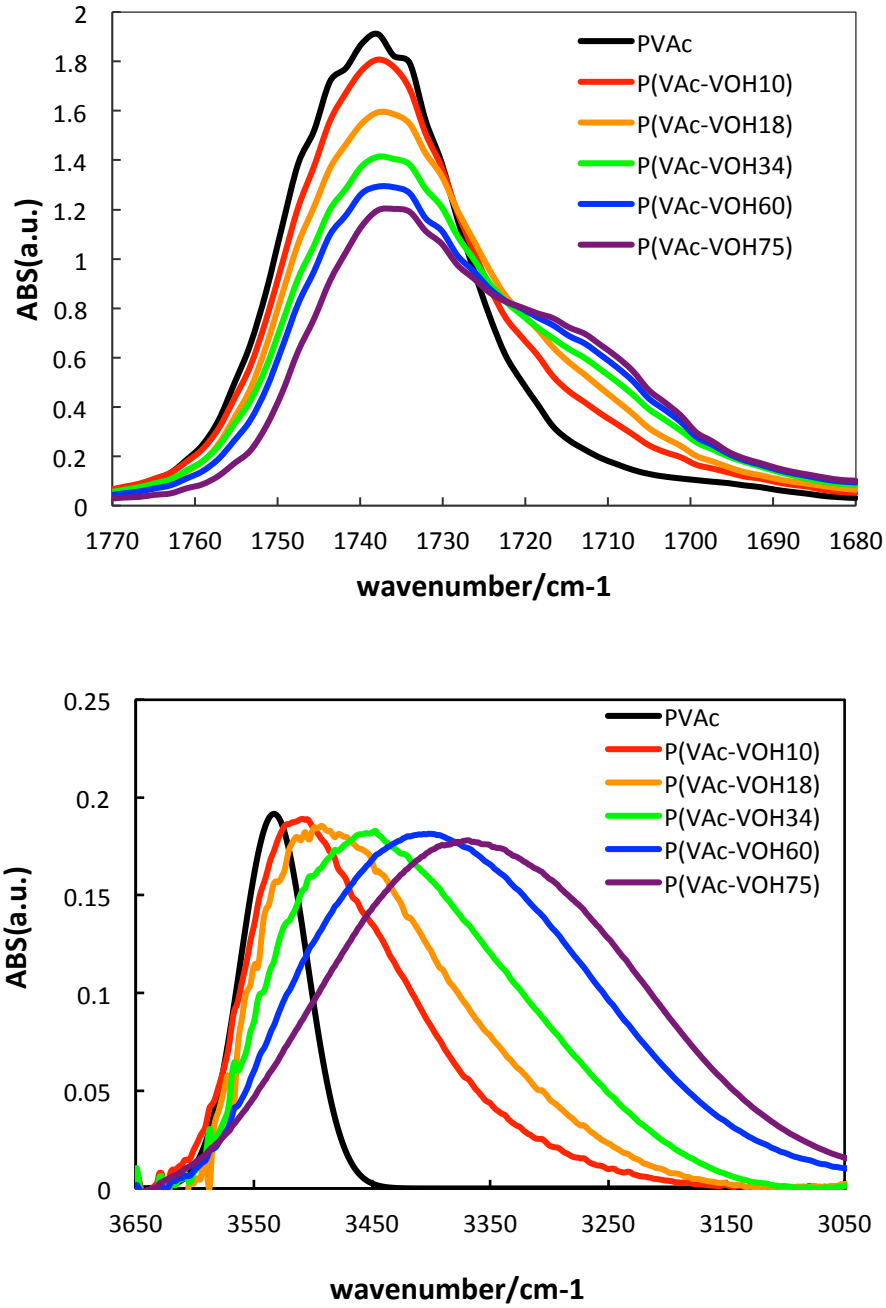

Figure 3.2 FT-IR spectra of (a) C=O stretching band, and (b) O-H stretching band in P(VAc-VOH)s.

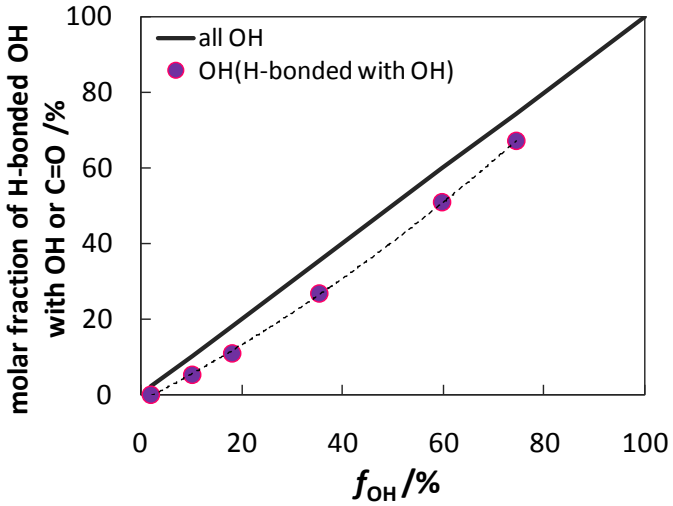

Figure 3.3 f_{OH} dependence of the fraction of hydrogen bonded OH.

3.3.2. Wide Angle X-Ray Scattering

Figure 3.4 shows the WAXS result of P(VAc-VOH) with f_{OH} = 2, 18, 34, 60, and 75%. Two amorphous hallo peaks appears for the samples of $f_{OH} \leq 34\%$. These two peaks locate at q=10nm^{-1} and 16nm^{-1}, probably corresponding to the nearest neighbor distances between the carbonyl groups and between the methylene and the methylene alcohol units, respectively. The low-q peak of P(VAc - VOH60) is unclear probably because of the low content of VAc units.

P(VAc-VOH75) showed well-defined diffraction peaks, indicating the PVOH crystals appeared. It can be said that the P(VAc-VOH) samples with $f_{OH} \leq 60\%$ are all amorphous.

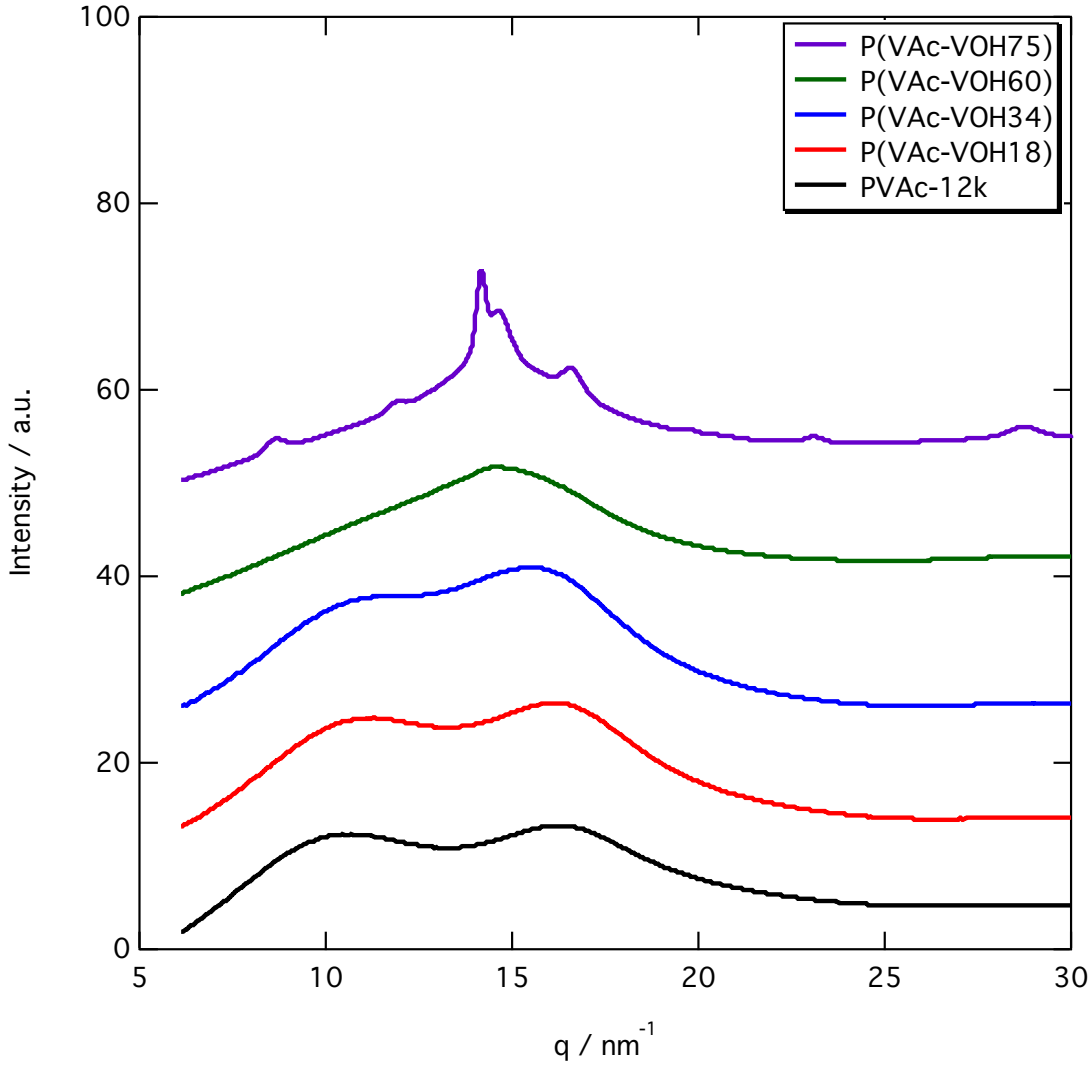

Figure 3.4 WAXS profiles of PVAc and P(VAc-VOH)s.

3.3.3. Small Angle X-Ray Scattering

Small angle X-ray scattering profiles of PVAc and P(VAc-VOH) are shown in Figure 3.5. Those data were measured at room temperature except for P(VAc-VOH75), whose data was obtained at T = 427K to avoid the effect of the crystallites. While no characteristic scattering profile is observed in P(VAc-VOH) with $f_{OH} \leq 18\%$, a shoulder appears in the range of 0.2~ 1nm^{-1} in P(VAc-VOH) with f_{OH}

= 34~75%, In this region the intensity, I, as a function of scattering angle, q, can be fitted by the Debye-Bueche (DB) equation:

$$I(q) = \frac{I(0)}{(1+\xi^2 q^2)^2} \tag{3.5}$$

Where $I(0)$ is the intensity at q=0 and ξ is the correlation length. These scattering profiles (represented by the DB equation) suggest the existence of the stronger correlation in the electron density than the system without specific interaction like polymer solution which will be represented by the Ornstein-Zernike(OZ) equation:

$$I(q) = \frac{I(0)}{1+\xi^2 q^2} \tag{3.6}$$

The correlation functions g(r) of the electron density fluctuation corresponding to the Fourier transform of the DB and the OZ equations are given by eqs 3.7 and 3.8, respectively.

$$g(r) \propto \exp(-r/\xi) \tag{3.7}$$

$$g(r) \propto \frac{\exp(-r/\xi)}{r} \tag{3.8}$$

The electron density correlations decay with the distance r in ways represented by these eqs. The shapes of the correlation functions are shown in Figure 3.6. It is seen that the correlation decay of OZ is faster than that of DB

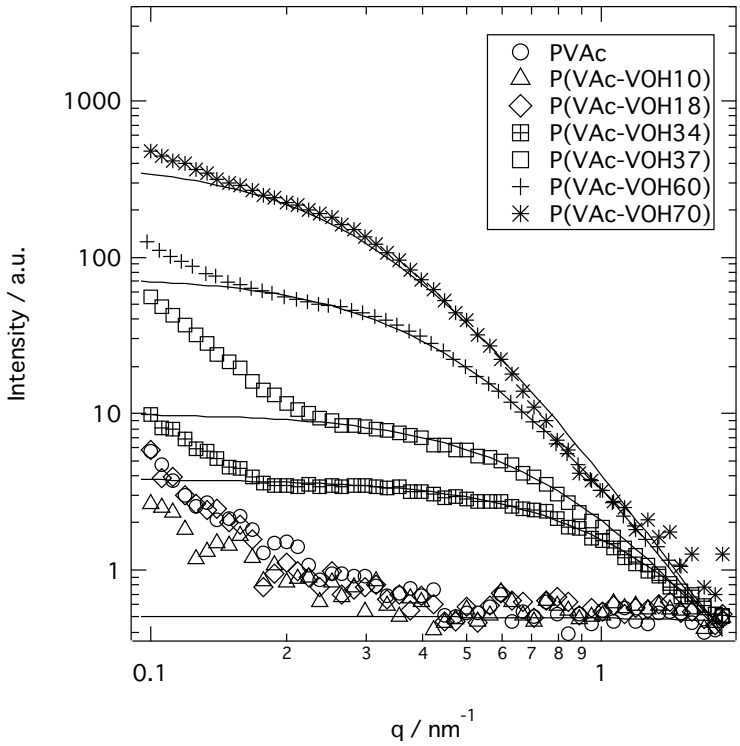

Figure 3.5 SAXS profiles of PVAc and P(VAc-VOH)s. Solid lines are fitting curves of Debye-Bueche equation.

.

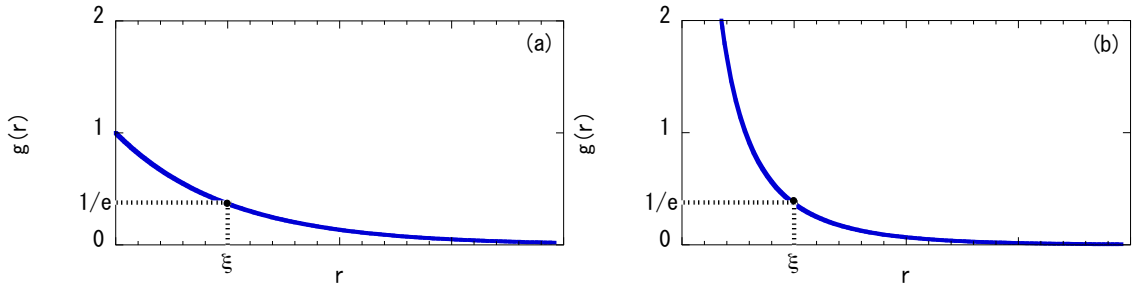

Figure 3.6 Autocorrelation function of (a) Debye-Bueche type and (b) Ornstein-Zernike type correlation.

The strong correlation represented by the DB function might be caused by the H-bonding interaction mainly formed between OH groups in P(VAc-VOH). Tashiro *et al.* also reported the DB type scattering profile for the Nylon in the melt state, in which

H-bonding interaction exists. I think the DB type scattering pattern will be specific to the H-bonding amorphous polymers. The ξ values obtained by the fitting of eq 3.5 are summarized in Table 3.2. The ξ values increase with f_{OH}, suggesting that the H-bonding interaction becomes stronger due to the aggregating H-bond for the higher f_{OH}.

Molecular weight dependence of $I(q)$ is shown in Figure 3.7. The shape of $I(q)$ is not dependent on M_w but dependent only on f_{OH}. Since the characteristic length scale ξ of the spatial inhomogeneity is around a few nm, which is smaller than the polymer chain dimension, I think ξ will be determined by the size of the local H-bonding aggregates of OH units, which can be a function of the spatial distance of OH units including sequential distribution in the copolymer chain and also the concentration of OH units. As a result, the scattering function will become independent of M_w.

3.3.4. Effect of the crystallization on the WAXS and SAXS profiles

The effect of the crystallization on the aggregation structure was examined. Figure 3.8 shows the WAXS and SAXS profiles for P(VAc-VOH75) measured at below and above the melting temperature (T_m=190°C). The sample was thermoformed at 200°C and cooled down to room temperature. WAXS and SAXS measurements were conducted on this sample at 25°C, and at 200°C. After that, the temperature was again dropped back to 25°C and WAXS and SAXS measurements were made again. As seen in Figure 3.7(b), the WAXS profile changes due to the melting and

recrystallization of the PVOH part. However, the SAXS profiles do not change so much.

Table 3.2 Correlation length ξ of P(VAc-VOH)s.

Sample code	ξ / nm
P(VAc-VOH34)	0.75
P(VAc-VOH37)	1.1
P(VAc-VOH60)	2.0
P(VAc-VOH75)	3.0
P(VAc-VOH34)-130k	0.75

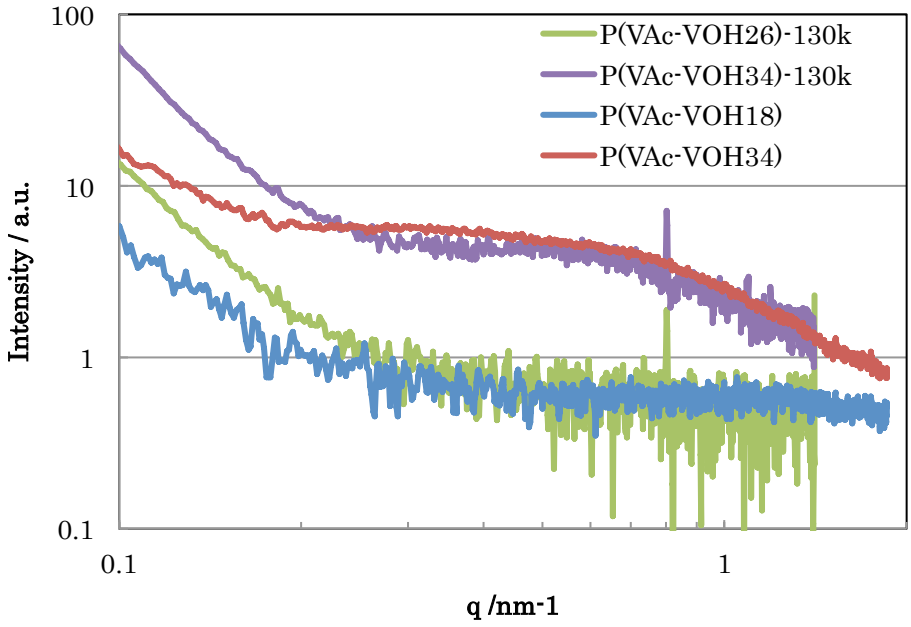

Figure 3.7 SAXS profiles of P(VAc-VOH)s of two molecular weight at 298K.

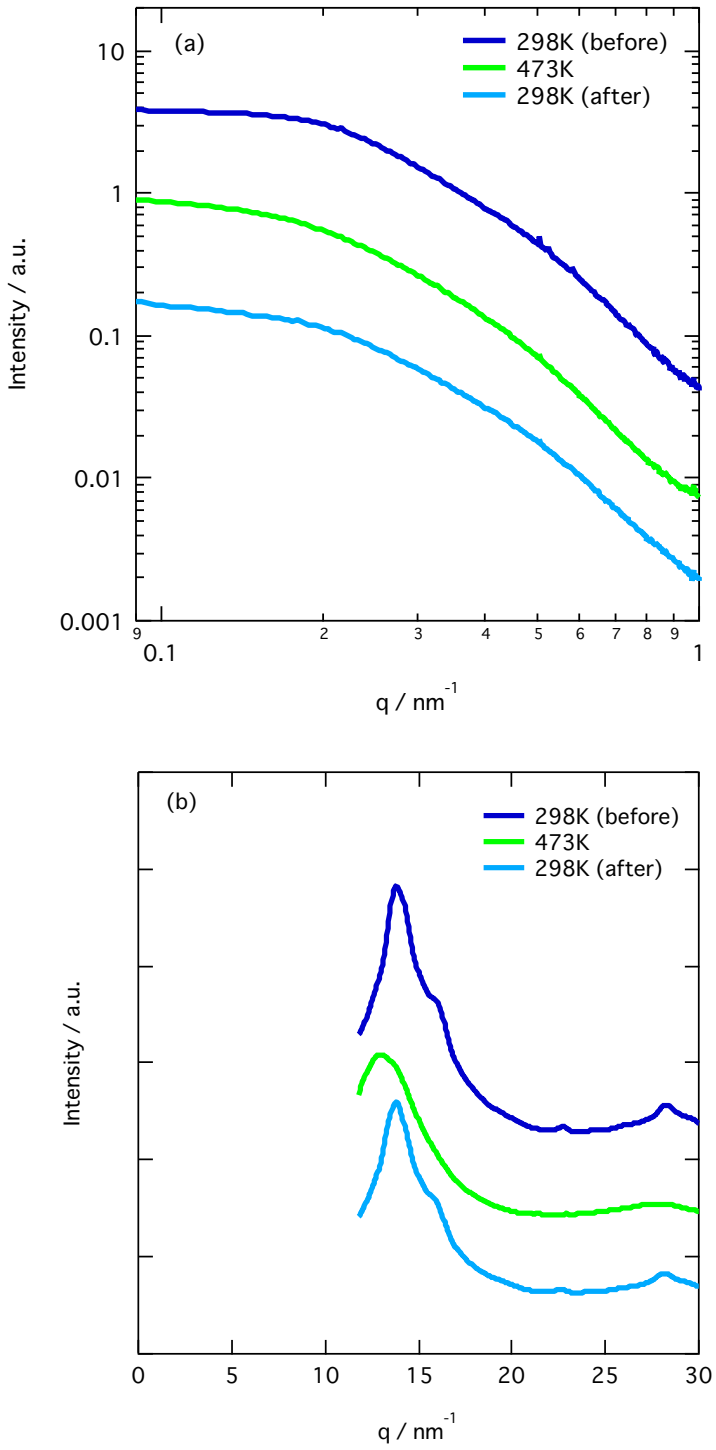

Figure 3.8 SAXS(a) and WAXS(b) profiles of P(VAc-VOH75) at 473K and RT after annealing in 473K.

Figure 3.8 indicates that the formation of the crystallites does not alter the nm scale inhomogeneous structure having scattering profile represented by the DB equation. This suggests that the preexisting H-bonded aggregation in the melt state is preserved inside the crystal and the aggregates do not change their size before and after the crystallization.

3.3.5. Viscoelastic property of P (VAc-VOH) in Flow Zone

Overview

Urakawa et al. reported the linear viscoelastic behavior of hydrogen bonding polymers, P(VAc-VOH).[10] In this section, I analyze their data based on the mean field percolation model in relation to the hyper-branched system described in the previous chapter.

Figure 3.9 shows the frequency, ω, dependence of the storage and loss modulus, $G'(\omega)$ and $G''(\omega)$, of P(VAc-VOH) with various f_{OH}, which is previously reported. Here, the method of reduced variables (temperature-frequency superposition principle) was used to construct the composite curve of G^* for each sample. The reference temperature, T_r, was 353 K. For the P(VAc-VOH60), the data at low ω were not superposed well, but for other samples the superposition principle worked well.

Since the molecular weight of P(VAc-VOH) is less than the characteristic molecular weight for entanglements, the $G'(\omega)$ spectra are compared with the Rouse model prediction represented by solid curves. $G^*(\omega)$ of the low f_{OH} samples are well described by this model. In contrast, $G^*(\omega)$ of the high f_{OH} samples ($f_{OH} \geq 35\%$)

deviate from the Rouse curve at low ω region. This will be due to the inter chain aggregation with long life time because the number of inter chain H-bonds increases with increasing the OH content. The rubbery plateau like region appeared in P(VAc-VOH60) (f_{OH} = 60%) at low frequencies, indicating the formation of network structure. Since the magnitude of the plateau modulus, G_N, decreases with increasing temperature, the cross-linking density of the network decreases with temperature. The effective molecular weight between the crosslinking points M_X is estimated by the rubber elasticity theory, $M_X \sim \rho RT/G_N$, where R is the gas constant and ρ is the density, as in the order of 10^6 at 150°C, which is about 100 times larger than the molecular weight of P(VA-OH). Therefore, the network strands are composed of over 100 polymer chains, and thus the effective cross-linking points are very scarce in this system. In addition, the frequency dependence of G' in the rubbery plateau region is broad and gradually decreases with decreasing the frequency. These features suggest that the associated structure with various sizes contributes to the response at the plateau region.

As discussed in the previous section, the Debye-Bueche type scattering profile appeared at $f_{OH} \geq 35\%$. In the rheological behavior deviation from the Rouse model appeared also at $f_{OH} \geq 35\%$. These results validate the speculation that inter chain aggregation with long life time is formed due to the multiple inter chain hydrogen bonding.

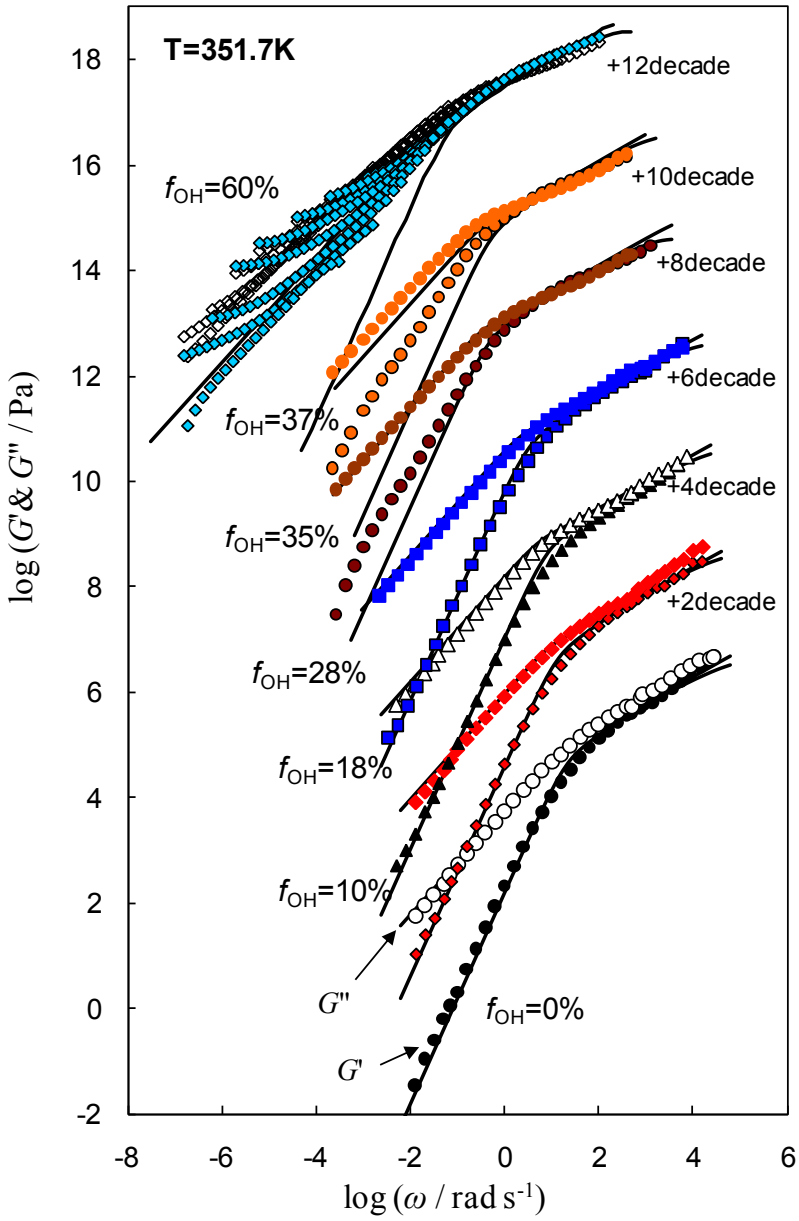

Figure 3.9 Storage and loss modulus for molten P (VAc-VOH) in the flow zone. These spectra were obtained by the method of reduced variables. The solid lines represent the Rouse mode prediction. The reference temperature is 352K.

Bond Percolation Theory on the Bethe Lattice

As a mean field model of gelation, a bond percolation on the Bethe lattice[11] is often used, which is shown in Figure 3.10. The Bethe lattice has the advantage of

directly taking into account the functionality of the monomers f by adopting this functionality of the lattice. All lattice sites are assumed to be occupied by monomers and the possible bonds between neighboring monomers are either formed with probability p or unreacted with probability 1-p.

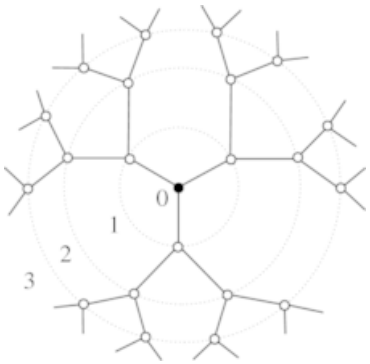

Figure 3.10 Bethe lattice with functionality f = 3 at p=1.

The sol-gel transition takes place at $p = p_c$ which is given by

$$p_c = 1/(f-1) \tag{3.9}$$

Near the gel point the number density of N-mers, $n(N)$, is written as

$$n(N) = \frac{f}{\sqrt{2\pi(f-1)(f-2)}}\, N^{-5/2}\, exp(-N/N^*)\,, \quad N^* = \{(f-1)p-1\}^{-2} \tag{3.10}$$

Here N^* is the cutoff (maximum) degree of polymerization. The parameters p, f, and N^* are not independent and the parameter to determine the shape of the distribution

function is either p or N^*, because the front factor involving f in the equation of $n(N)$ can be neglected by the normalization process. Note that the mean field type distribution function given by eq 3.10 is different from that for the case of hyperbranched polymers given by eqs 2.5 or 2.6 in Chapter 2: The power index to the molecular weight (or degree of polymerization) is -3/2 for the hyperbranched polymer described in chapter 2 but -5/2 in the case of the mean field.

Considering the crosslinking of long linear precursor chains with degree of polymerization N_0 and functionality f (>>1) in the melt. This class of gelation is called vulcanization, named after Goodyear's famous process to crosslink natural rubber using sulphur. Vulcanization is known to be one type of gelation for which the mean-field theory works well.[11,12] If a single precursor chain with many bonding sites occupies a single site of the Bethe lattice, the functionality f becomes very large and the critical gel point is very low according to eq 3.9. In this case all the deviations from the mean field theory, such as the loop formation and excluded volume effect become negligible.

Viscoelastic spectra for associative branching chains can be calculated by using the number density distribution function $n(N)$ and the Rouse model, if the dynamics of all the associated chains with different sizes are independent and entanglement effect does not appear.

$$G^*(\omega) = \frac{\sum_{N=1}^{N^*} n(N) \frac{\rho RT}{N_0 m} \sum_{p=1}^{N_0 N} \frac{\omega^2 \tau_p^2 + i\omega\tau_k}{1+\omega^2\tau_k^2}}{\sum_{N=1}^{N^*} N\, n(N)} \tag{3.11}$$

$$\tau_k = \tau_s \left(\frac{N_0 N}{k}\right)^{(1/\nu+2)/3} = \tau_1 \left(\frac{N}{k}\right)^{(1/\nu+2)/3} \tag{3.12}$$

Here N_0 is the degree of polymerization, m is the molar mass of the repeating unit, τ_s and τ_1 are the shortest and the longest relaxation times of the precursor polymer, respectively. Eq 3.12 is the same with eq 2.18 in the previous chapter. In the case of the branched chain on the Bethe lattice (the mean field), the fractal dimension (=$1/\nu$) is known to be 4 and the space dimension to be 6. This means ν=0.25 in eq 3.12, and thus the Rouse type scaling $\tau_k \sim k^{-2}$ holds.

In the molten P(VAc-VOH), H-bonds between OH groups becomes dominant for the higher f_{OH} and cause the inter-chain association. Therefore, this system can be regarded as the case of "vulcanization" and mean filed theory might work well. Figures 3.10 (a)-(d) and 3.11 (a)-(c) show the fitting results by the mean field theory of the G^* data of P(VAc-VOH) with several OH contents f_{OH}. As well known for the pure PVAc (without specific inter-chain interaction), the Rouse model (N^* = 1) can fit the data fairly well with one parameter τ_1 (=0.03s). In the case of f_{OH}=10%, the simple Rouse model fitting was also possible with the τ_1 value determined based on the T_g difference. However, for the f_{OH}= 18% and 28%, it was necessary to increase the cutoff aggregation number N^* in order to fit the data. N^*=2 and 3 for f_{OH}= 18% and 28%, respectively, gave good agreements. That is to say, viscoelastic spectra for the samples with f_{OH} less than 28% can be expressed in terms of the mean field aggregation model given by the eqs 3.10-3.12 with taking into account the T_g difference. On the other hand, in the case of $f_{OH} \geq 35\%$ these equations did not give good-fits to the data. The deviations were seen in the following points:

(1) The τ_1 values determined from the T_g data were too short and were necessary to be replaced by τ_1* whose values are given in the figures.

(2) The Rouse type scaling $\tau_p \sim p^{-B}$ (with $B = 2$) corresponding to the high frequency power law $G'(\omega) \sim G''(\omega) \sim \omega^{1/B}$ slightly deviates upward from the G* data, so that the B values were changed to give better fits. Those B values are also shown in the figures.

(3) In the low frequency region, addition of extra relaxation mode to the eq 3.11 was necessary to fit the data. The extra mode was simply represented by the Maxwell model given by eq 3.13.

$$G^*(\omega) = \frac{G_D\omega^2\tau_D^2}{1+\omega^2\tau_D^2} + i\frac{G_D\omega\tau_D}{1+\omega^2\tau_D^2} \qquad (3.13)$$

As discussed in the previous section, the inter-chain H-bonding force becomes stronger and SANS profiles change at $f_{OH} \geq 35\%$, so that the behaviors of (1)~(3) will be correlated to the structural change. We think (1) and (2) are related to the emergence of the entanglement effect. Lusignan et al. reported the decrease of the power law exponent (~1/B) near the critical point when the entanglement effect appears,[13] which is in harmony with the increase in B values shown in Figure 3.11. Concerning the behavior of (3), we think that the dissociation of the aggregates will be responsible for the extra relaxation mechanism observed at low frequencies. Rubinstein and Semenov[14] predicted the appearance of the Maxwell type relaxation corresponding to the life time of temporary network structure. By looking at this extra

relaxation modes, the intensity G_M is increased by increasing the OH contents possibly due to enforcement of the inter-chain association. The relaxation time τ_M corresponding to the life time of the association also increases with increasing the OH content probably due to the formation of multiple H-bond.

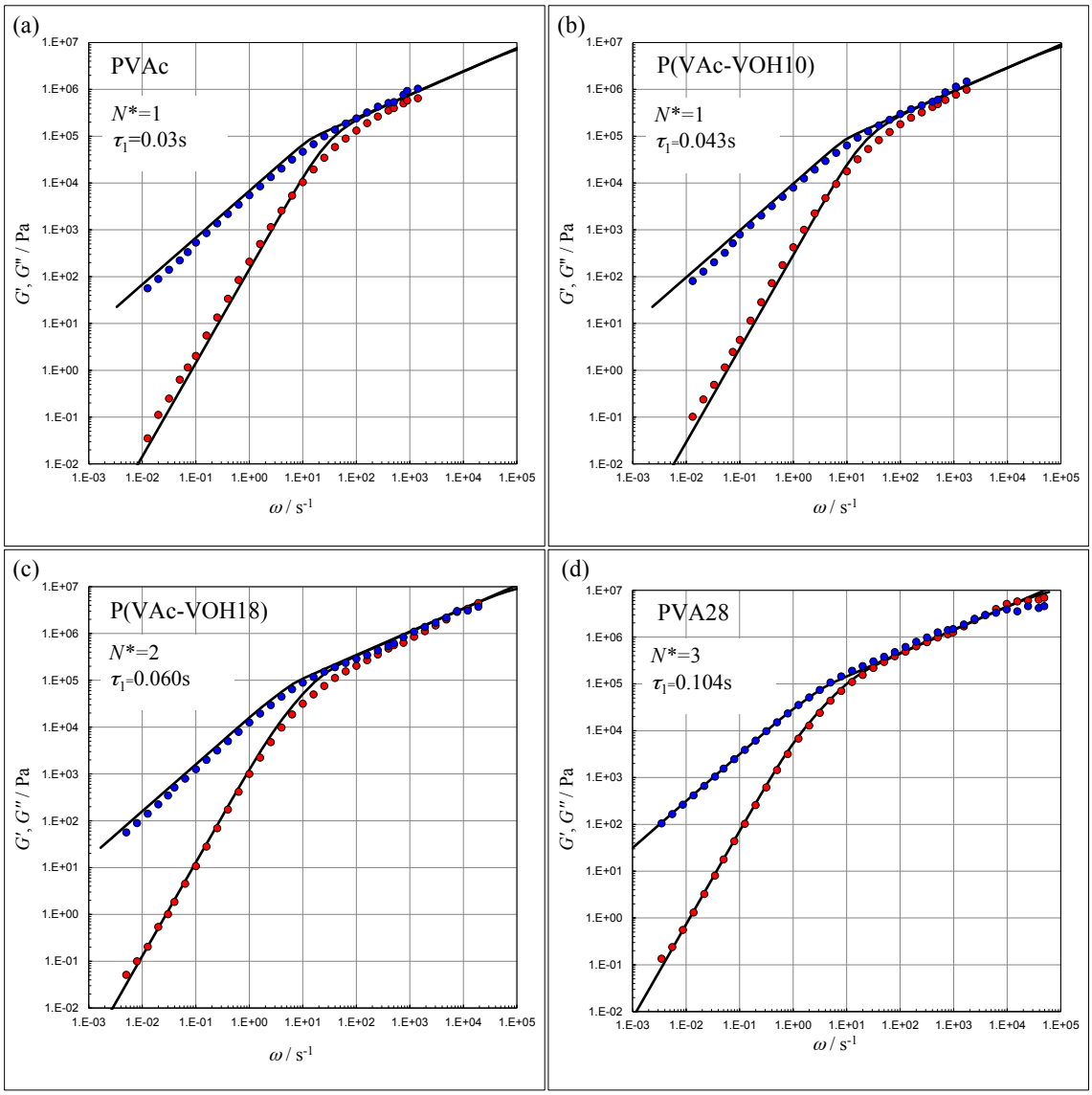

Figure 3.11 Complex moduli for PVAc (a), and P(VAc-VOH) with f_{OH} =10% (b), 18%(c), and 28%(d). The solid curves are the fitted results with eqs 3.10-3.12.

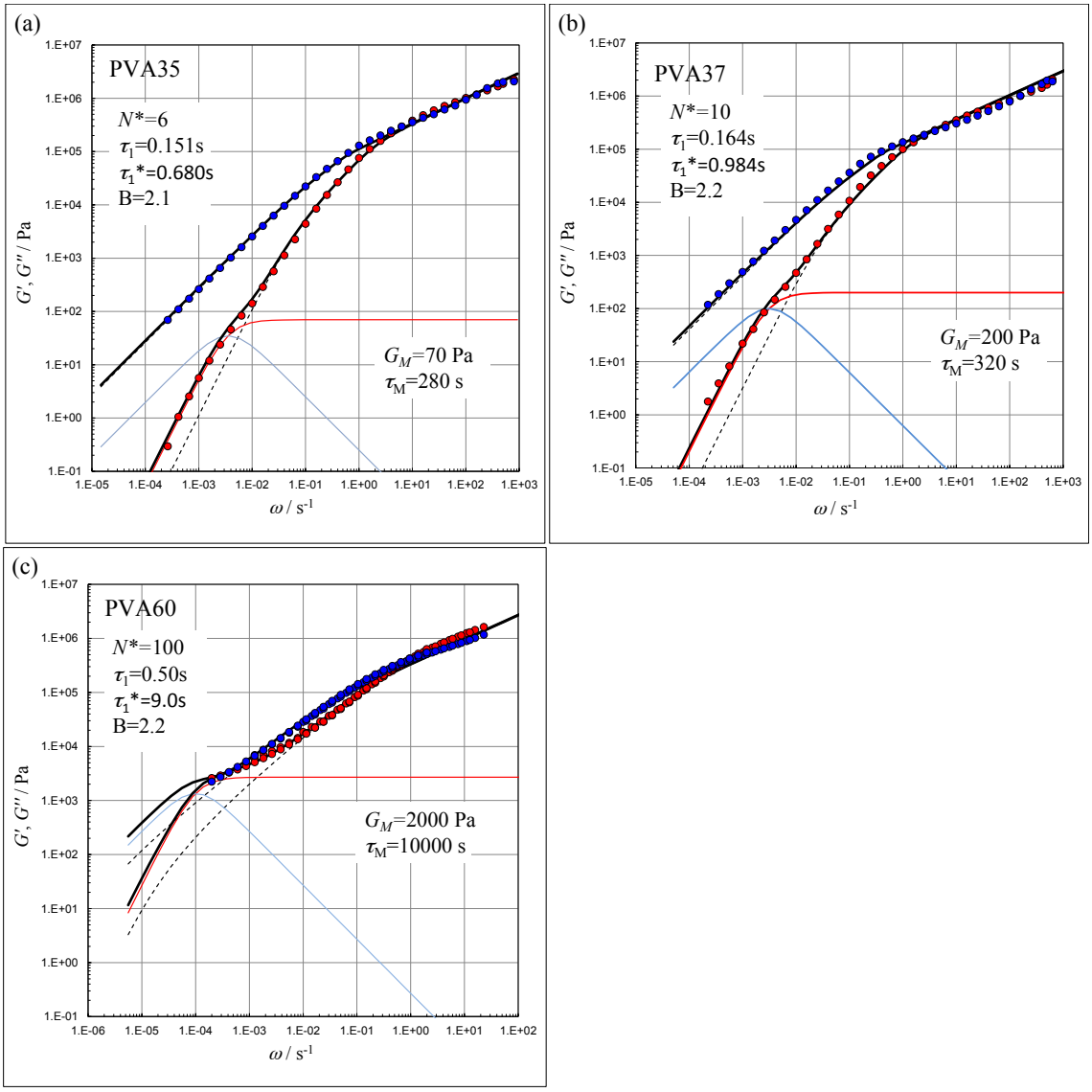

Figure 3.12 Complex moduli for P(VAc-VOH)s with f_{OH} =35% (a), 37% (b), and 60% (c). The dashed curves are the fitted results with eqs 3.10-3.12. Red and blue solid lines represent the Maxwell relaxation of *G*' and *G*"

3.4. Conclusion

FTIR measurements revealed that two types of hydrogen bonds between OH···OH and C=O···HO were formed in the amorphous P(VAc-VOH)s. As the increase of f_{OH}, OH···OH H-bonds became dominant.

SAXS profiles of the amorphous P(VAc-VOH)s could be fitted by the Debye-Bueche equation, indicating that the stronger composition correlation exists compared with the general composition fluctuation usually observed miscible blends. This stronger correlation was concluded to be due to the H-bonding between OH···OH. The correlation length ξ was enlarged by increasing the number of hydrogen bonds. The ξ values were not dependent on the molecular weight of copolymers but on only the f_{OH}.

For P(VAc-VOH75), which crystallize below 190°C, the nm-size inhomogeneous structure characterized by the Debye-Bueche type scattering profile, did not change even when the polymers were crystallized. This suggests that the structure of the local H-bonded aggregates formed in amorphous state is preserved upon crystallization.

Viscoelastic behavior was analyzed for a series of P(VAc-VOH) samples in the melts based on the mean field random branching theory. At $f_{OH} \leq 28\%$, all the data could be described by the mean field theory. At $f_{OH} \geq 35\%$, deviation from the theory was observed. Concerning the discrepancy, three points were raised: (1) shorter relaxation time (τ_1) of the precursor chain, (2) smaller power law exponent ($1/B$) in $G^*(\omega)$ at the high frequency region compared to the Rouse model ($1/B$=0.5), and (3) appearance of the extra-relaxation in $G^*(\omega)$ at the low frequency region. (1) and (2) were explained to be due to the entanglement effect. For the (3), I proposed the possibility that the dissociation of the H-bonded chains might be responsible.

3.5. References

1. Urakawa, O.; Ikuta, H.; Nobukawa, S.; Shikata, T., *Journal of Polymer Science Part B: Polymer Physics* **2008**, 46 (23), 2556-2565.
2. Minsk, L. M.; Priest, V. J.; Kenyon, W. O. *J. Am. Chem. Soc.* **1941**, 63, 2715.
3. Isasi, Jose R., Luis C. Cesteros, and Issa Katime. *Macromolecules,* **1994**, 27 (8), 2200-2205.
4. Moritani, T.; Fujiwara, Y; *Macromolecules* **1977**, 10 (3), 532-535.
5. Bunn, C. W.; *Nature* **1948**. 161 (4102), 929-930.
6. Roe, Ryong-Joon, and R. J. Roe. *Methods of X-ray and neutron scattering in polymer science.* Oxford University Press: New York, **2000**.
7. Debye, P.; Bueche, A.; *Journalof Applied Physics* **1949**. 20(6), 518-525.
8. Ornstein, L. S.; Zernike, F.; *Accidental deviations of density and opalescence at the critical point of a single substance.* Proc. Acad. Sci. Amsterdam. **1914**.
9. Tashiro, K.; Nishiyama, A.; Tsuji, S.; Hashida, T.; Hanesaka, M.; Takeda, S.; Weiyu, C.; Reddy, K. R.; Masunaga, H.; Sasaki, S.; *Journal of Physics: Conference Series, IOP Publishing*. **2009**. p 012002.
10. Urakawa, O.; Shimizu, A.; Inoue, T. submitted to Soft Matter.
11. Rubinstein, M.; Colby, R. H., *Random branching and gelation. In Polymer Physics*, Oxford Universiyt Press: **2003**, 199-252.
12. De Gennes, P. G., *Scaling Concepts in Polymer Physics*, Cornell University Press; **1979**.
13. Lusignan, C. P.; Mourey, T. H.; Wilson, J. C.; Colby, R. H.; *Physical Review E.*

1999. 60 (5), 5657-5669.

14. Rubinstein, M.; Semenov, A. N.; *Macromolecules* **1998**, 31 (4), 1386-1397.

Chapter 4 Viscoelastic Properties and Birefringence of Phenolic Resins

4.1. Introduction

Phenolic resins are the earliest commercial synthetic resin and used for various applications, for example, circuit boards, mold products, adhesives and so on. [1, 2, 3] Phenolic resins are thermo-setting plastics, and they are neither soluble in solution nor melted after subjected to cure reactions. For this reason, the characterization methods for phenolic resins are very limited, and therefore the relationship between mechanical property and structure of phenolic resins are not well-understood. Usually, cure reactions are characterized by thermal or spectroscopic measurements. Thermal measurement enables to know the curing ratio by heat of reaction. The residual ratio of functional group of resins or cure agents is determined by spectroscopy. However the chemical reaction of phenolic resins is not clearly understood, because polymerization process and thermodynamics of phenolic resins are very complicated. Therefore, thermal and spectroscopic measurements have been utilized to qualitatively only estimate cross-link density of phenolic resins.

For linear polymers, molecular origin of stress in the rubbery state can be described with the coarse graining molecular model. [4] In the model, the chain is divided into viscoelastic segments. The rubbery stress can be related with the anisotropic chain conformation and therefore it can be described with the orientation of segments. This molecular picture is supported by the stress-optical rule. [5] The viscoelastic segment of

polystyrene is composed of about ten repeating units.[6] On the other hand, thermo-setting plastics form highly cross-linked network structures, and sometimes the strand between two cross-linking points can be smaller than the viscoelastic segment size. Thus, the viscoelastic property of the highly cross-linked polymer cannot be described with ordinary coarse graining molecular models.

Another complication of the phenolic resins is inhomogeneous network structure. Usually, crosslinking reaction of the phenolic resins progresses inhomogeneously and the resulting network structure becomes inhomogeneous. Crosslinking density is not uniform in the system.

In this study, we measured viscoelastic properties and strain-induced birefringence of the phenolic resins with various degrees of cross-linking around the glass transition region to clarify the molecular origin of stress for highly cross-linked networks.

4.2. Experimental

We used phenolic moldings of random novolac (NV) purchased by Sumitomo Bakelite Co., Ltd as phenolic resin and 1,3,5,7-tetraazatricyclo(3.3.1.1 (3,7)) decane (Hx: hexamethylenetetramine) purchased by CCP Co., Ltd as cure agent. The random novolac sample was identical with the sample RN7200 used in Chapter 2. The chemical structure of NV and Hx are shown in Figure 4.1. As mentioned in Chapter 2, the weight averaged molar mass, M_w, and the number averaged molar mass, M_n, of the random novolac were measured as M_w=4.4 x 10^3 gmol^{-1} and M_n=9.5 x 10^2 gmol^{-1} with a gel

permeation chromatography (GPC) (Tosoh) and Right Angle Light Scattering (RALS)/Visco detector (TDA302; Viscotek). Degrees of cross-linking of phenolic moldings were changed by amount of cure agent 1.6 ~ 6.0 wt %, the sample codes of phenolic moldings are named as "Hx/NV-" and amount of cure agent. T_g of samples are measured by modulated DSC (DSC2910, TA Instrument). Results of the DSC measurements are shown in Figure 4.2 and Table 4.1. T_g increased with increasing of amount of the cure agent.

Viscoelastic and birefringence properties of phenolic resins are measured by a tensile type rheometer (Rheospectoler DVE 3, Rheology Co., Ltd.) attached with an optical systems at several temperatures between T_g – 30K and T_g + 30K in the frequency range of 1-130 Hz. Details of the apparatus were published elsewhere. [6] A home-built apparatus of shear measurements were utilized for measurement of the random novolac. Details of the shear apparatus have already been reported.[7, 8] The measurement mode of viscoelasticity and birefringence are summarized in Table 4.1.

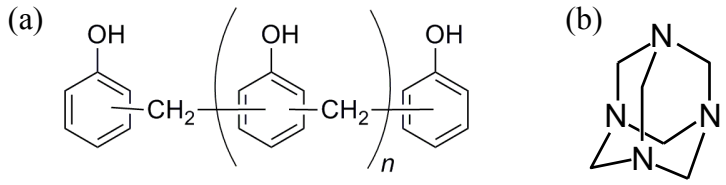

Figure 4.1 Chemical structures of (a) novolac and (b) cure agent (hexamethylene-tetramine).

Table 4.1 Composition and T_g of phenolic resins

Sample Name	wt% of cure agent	T_g/K	Cure Reaction	test mode
Random Novolac	0	306	none	shear
Hx/NV-1.6	1.6	356	175°C/6h	tensile
Hx/NV-2.2	2.2	367	175°C/6h	tensile
Hx/NV-3.1	3.1	382	175°C/6h	tensile
Hx/NV-6.0	6.0	444	175°C/6h	tensile

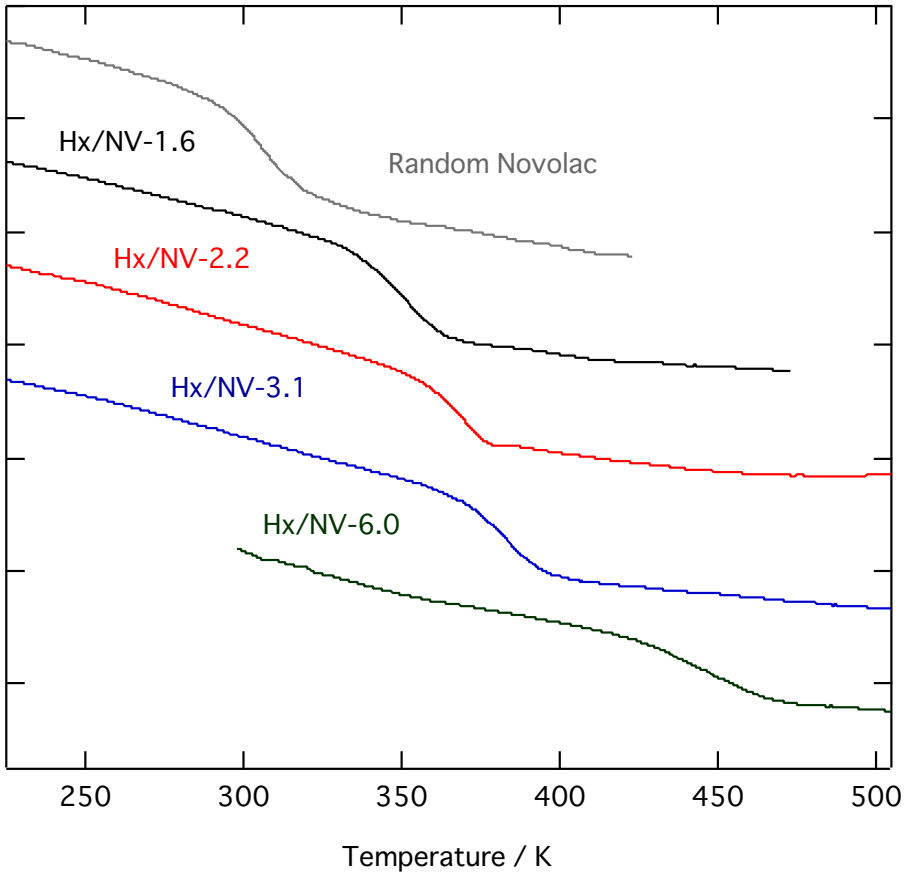

Figure 4.2 Differential scanning calorimetry of phenolic resins.

4.3. Results

Figure 4.3 shows the complex shear modulus, $G^*(\omega)= G'(\omega)+iG''(\omega)$, and the complex strain-optical coefficient, $K^*(\omega)= K'(\omega)+iK''(\omega)$, which is the complex ratio of shear birefringence component, n_{12}, of refractive index tensor to the strain, of the random novolac at the reference temperatures, 393K. The relationship between birefringence and stress of amorphous polymers can be written with the modified stress-optical rule, MSOR.[6] MSOR says that both the stress and birefringence have two components, rubbery and glassy components. The rule for shear quantities can be express as follows.

$$G'(\omega)=G'_R(\omega)+G'_G(\omega) \quad (4.1)$$

$$K'(\omega)= K'_R(\omega)+K'_G(\omega) =C_R\, G'_R(\omega)+ C_G\, G'_G(\omega) \quad (4.2)$$

Here, the subscript denotes R, rubbery and G, glassy components. In a previous study on random novolacs, we determined $G^*_R(\omega)$ and $G^*_G(\omega)$ and showed that random novolacs have randomly branched structure.[9] The stress-optical coefficient, C_R, was estimated to $2.2\times10^{-9}Pa^{-1}$. C_R of bisphenol A polycarbonate, a linear polymer having similar molecular structure to novolac, is $5.0\times10^{-9}Pa^{-1}$. [10] The small C_R value of novolacs suggests that the novolacs have a relatively flexible chain structure. Accordingly, the estimated viscoelastic segment size of novolacs was 300 $gmol^{-1}$ as mentioned in Chapter 2.

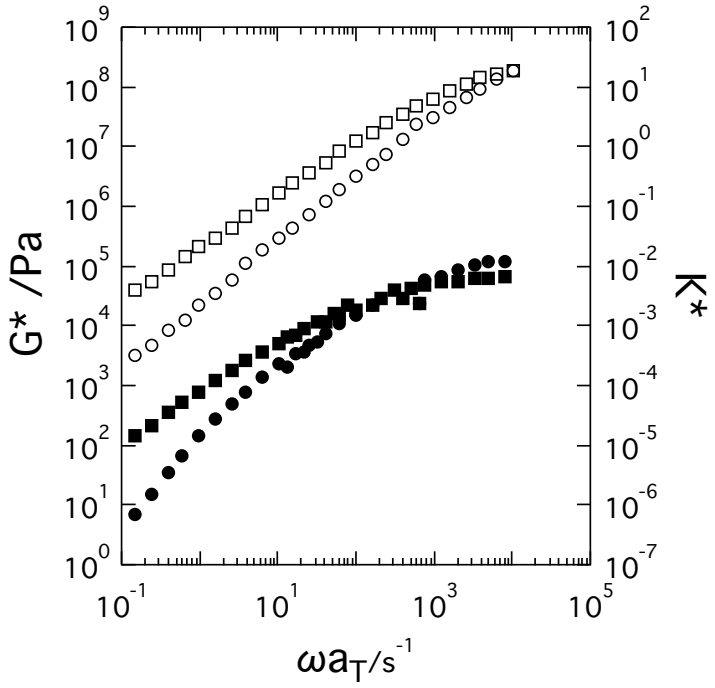

Figure 4.3 Viscoelastic properties and birefringence of random novolac. Opened symbols are complex shear modulus and closed symbols are complex strain-optical coefficient; circle and square symbols are real and imaginary part of G^* and K^*, respectively. Reference temperature is 373K. The G^* in this figure is same as Figure 2.13, but only reference temperature is difference. (The reference temperature of Figure 2.13 is 353K.)

4.3.1. Overview of E^* and O^* of phenolic resins

Figure 4.4 shows the complex Young's modulus, $E^*(\omega)= E' + iE''$and the complex stress-optical coefficient in tensile deformation, $O^*(\omega)=O' + iO''$, of the four phenolic resins with different degrees of cross-linking at the reference temperature, $T_r \sim T_g + 10$K. Here, the method of reduced variables [11] was used to obtain the composite curve. The temperature-frequency superposition worked well although the breakdown of the method of reduced variables was reported for various polymers around the glass-to-rubber transition zone.

Around the glass transition zone, Young's modulus and stress-optical coefficient of Hx/Nv-1.6 relax about two decades in magnitude. Young's moduli of Hx/NV-2.2, Hx/NV-3.1 and Hx/NV-6.0 relax about one decade in magnitude irrespective of cross-linking density. On the other hand, the complex strain-optical coefficient strongly depends on the cross-linking density. The low cross-linking phenolic resins, Hx/NV-1.6 and 2.2, show that the shape of O^* is almost the same as E^*, but the relaxation magnitude of O^* decreases with increasing of the cross-linking density. Since birefringence mostly reflects the orientation of benzene rings having large anisotropy in phenolic resins, the present results show that the reorientation of phenolic groups around the glass transition zone are restricted with increasing the cross-linking density. Young's modulus of Hx/NV-1.6 shows two step-wise relaxation as indicated by arrows, while O^* relaxes in a single process. The two step-wise relaxation suggests the system is not homogenous. This issue will be discussed later.

Next, I determined the characteristic quantities of cross-linking structure. We can define the limiting values for E' at high and low frequencies, $E'(\infty)$ and $E'(0)$. $E'(\infty)$ corresponds to the limiting glassy modulus, and $E'(0)$ corresponds to the plateau modulus, E_N, of phenolic resins. Similarly, we define the limiting values for O', $O'(\infty)$ and $O'(0)$. For example**,** $E'(\omega)$ for Hx/Nv-1.6 gradually decreases with decreasing of frequency in the low frequency range, and the $E'(0)$ value is not clear in double logarithmic scales. Thus, we extrapolated $E'(\omega)$ at ω=0 in a linear plot. The typical experimental uncertainty of the limiting values is 10%. The obtained values are summarized in Table 2. The stress-optical coefficient in the rubbery zone can be

estimated with C_R=O'(0)/ E'(0). C_R values of phenolic resins are smaller than C_R of no-crosslinking random novolac and C_R values decreases with increasing of crosslinking density, in spite of C_R of amorphous polymers is determined by the anisotropy of polarizability of segments. The present result strongly suggests that E'(0) is not determined by the simple rubber network theory.

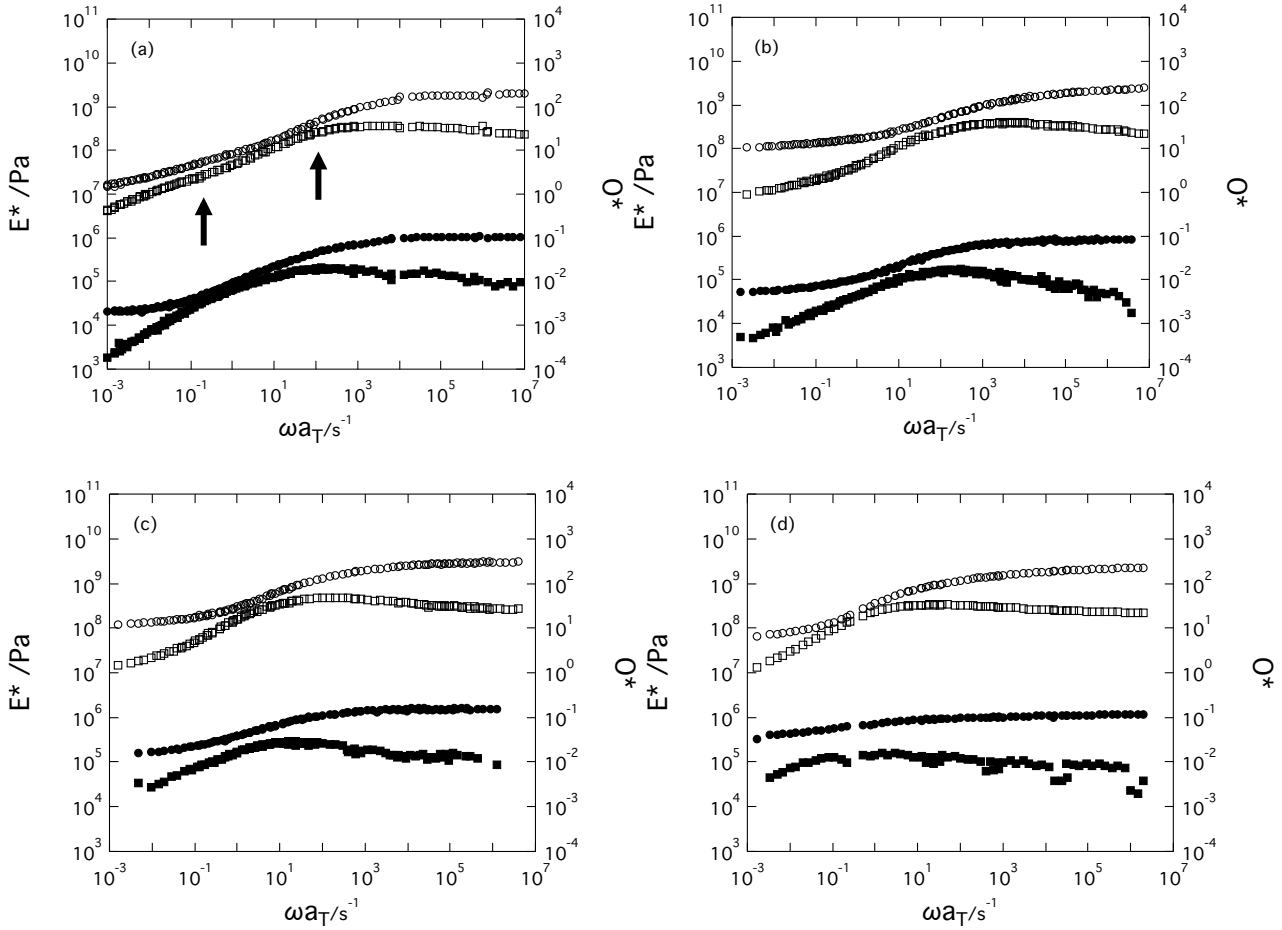

Figure 4.4 Viscoelastic properties and Birefringence of Phenolic resins, (a)Hx/Nv-1.6, (b)Hx/Nv-2.2, (c)Hx/Nv-3.1, (d)Hx/Nv-6.0. Opened symbols are complex Young's modulus and closed symbols are complex strain-optical coefficient; circle and square symbols are real and imaginary part of E^* and O^*, respectively. Reference temperatures are (a)368K, (b)377K, (c)393K, (d)453K, respectively.

Table 4.2 Characteristic parameters for phenolic resins.

	$E'(0)$ /GPa	$E'(\infty)$ /GPa	$O'(0)$	$O'(\infty)$	C_R /10^{-10}Pa^{-1}	C_G /10^{-11}Pa^{-1}	$O_R'(\infty)$	M_C[a] /gmol^{-1}
Random Novolac	N.A	2.0	N.A.	0.1	2.2	3.7	0.02	N.A
Hx/NV-1.6	0.02	2.0	0.0022	0.11	2.1	4.0	0.05	5900
Hx/NV-2.2	0.10	2.7	0.0060	0.085	0.53	2.5	0.03	1200
Hx/NV-3.1	0.11	3.0	0.015	0.15	1.3	3.6	0.07	900
Hx/NV-6.0	0.055	2.2	0.030	0.12	5.5	3.2	0.05	520

[a] Estimated from eq. 4.11

4.3.2. Estimation of molar mass of network strands from rubber-elasticity.

The molar mass of the network strand between crosslinking points, M_C, has been estimated by the follow equation on the assumption of rubber elasticity. [12]

$$M_C = \frac{\rho RT}{G_N} = \frac{3\rho RT}{E_N} = \frac{3\rho RT}{E'(0)} \tag{4.3}$$

Here, we assume E_N=3G_N. However, if we applied eq. 4.3 to the present data, we obtain unrealistic results. The estimated molar mass of the network strand of Hx/NV-1.6 is about 1000 g mol^{-1}. On the other hand, Hx/NV-2.2, 3.1 and 6.0 show the estimated molar mass of network strand is about 100 g mol^{-1}. This value is close to the molecular weight of phenol and methylene monomers, 108 g mol^{-1}, clearly indicating that the traditional theory for rubber elasticity cannot be applied. As we have described earlier, the M_w of viscoelastic segments of the uncrosslinked sresin was 300 g mol^{-1}. Thus, we cannot estimate the correct M_C value from the rubbery plateau modulus. As we have seen already, C_R varies with the crosslinking density. The unrealistic small M_C values

consistently indicate the breakdown of rubber elasticity. I will show that the network structure can be characterized the birefringence data.

4.3.3. The relationship between birefringence and stress.

The relationship between strain-induced birefringence and stress can be written with the modified stress-optical rule, MSOR,[13] in ordinary amorphous polymers. The MSOR for tensile deformation can be written as follows.[6]

$$E'(\omega)=E'_R(\omega)+E'_G(\omega) \tag{4.4}$$

$$O'(\omega)= O'_R(\omega)+O'_G(\omega) =C_R\, E'_R(\omega)+ C_G\, E'_G(\omega) \tag{4.5}$$

The MOSR is based on the SOR in the rubbery zone. In the rubber zone, the glassy component relaxes completely and therefore $E'_G(\omega) \rightarrow 0$ and $E''_G(\omega) \rightarrow 0$. Thus, eqs. 4.4 and 4.5 reduces the ordinary SOR, $O^*(\omega)=C_R\, E^*(\omega)$. However, as we have discussed earlier, the SOR does not hold valid for phenolic resins. One possible explanation for the breakdown SOR is the existence of the third component in the rubbery region. As we have already pointed out, Young's modulus of Hx/NV-1.6 shows two step relaxations (see Figure 4.4). This feature strongly suggests the relationship between birefringence and stress cannot be described with two components version of MSOR. We speculate that additional relaxation process would be necessary to describe the stress-birefringence relationship. This is probably due to their inhomogeneous structure. In the following section, I analyze O^* in detail. This is because the birefringence mainly

reflects the reorientation of segments and therefore the analysis would be easier than the stress relaxation.

4.3.4. Estimation of cross linking density from birefringence data.

The orientational birefringence is related with the intrinsic birefringence, Δn_0, and orientation degree of repeating units, f.

$$\Delta n = \Delta n_0 f \tag{4.6}$$

We can estimate f from the birefringence by using eq. 4.6. MSOR says that birefringence includes not only the orientational birefringence (R component) but also the glassy component, O_G^* in the glass zone. The contribution of O_G^* may be estimated as below. In the following, we ignore details of frequency dependence of O_G^*, and we just discuss about the limiting behavior at high and low frequencies. At high frequencies, MSOR can be written as follows.

$$O'(\infty) = O'_R(\infty) + O'_G(\infty) = O'_R(\infty) + C_G E'_G(\infty) \tag{4.7}$$

To the best of our knowledge, C_G of the polymers containing benzene rings is an almost constant value of 3×10^{-11} Pa^{-1}, irrespective of the molecular structure of the repeating unit, and $E'_G(\infty) \sim E'(\infty)$ is approximately 2×10^9 Pa for the present phenolic resins. Thus, we can estimate $O'_G(\infty)$ value from $C_G E'_G(\infty)$. Now, $O'_R(\infty)$ value can be

estimated as $O'(\infty)$–$O_G'(\infty)$. The determined values are summarized in Table 2. The $O'_R(\infty)$ value related with the molar mass of viscoelastic segment, M_S of phenolic resins.[6, 13]

$$M_S = \frac{\rho RT}{G_R'(\infty)} = \frac{3\rho RT}{E_R'(\infty)} = \frac{3C_R\rho RT}{O_R'(\infty)} \tag{4.8}$$

The glassy component would have relaxed in short times in the low frequency range, and therefore we obtain

$$O'(0) = O'_R(0) \tag{4.9}$$

The $O'_R(0)$ value related with the molar mass of network strand.

$$M_C = \frac{\rho RT}{G_R'(0)} = \frac{3\rho RT}{E_R'(0)} = \frac{3C_R\rho RT}{O_R'(0)} \tag{4.10}$$

For the case of phenolic resins, $E'(0) >> E'_R(0)$ and therefore, eq. 4.3 provides unrealistic M_C value. On the other hands, we anticipate that $O'(0)=O'_R(0)$ holds well. Comparing eqs 4.8 with 4.10, molar mass of the network strand between the crosslinks, M_C, may be estimated by the following equation.

$$M_C = M_S \frac{O'_R(\infty)}{O'_R(0)} \tag{4.11}$$

In the above discussion, we used the SOR. However, the validity of the SOR is not essential. Since the birefringence can be related with orientational degree of structure units, as described with eq. 4.6, the ratio, $O'_R(0)/ O'_R(\infty)$, can be regarded as the relaxation ratio of orientation, $f(0)/f(\infty)$. According to the molecular theory, the relaxation of segment orientation relates to the increase of size of subchain.[14] The estimated value of M_C from the birefringence relaxation is summarized in Table 4.2. M_C decreases with increasing of crosslinking density as we expected.

The concentration of network strand can be estimated from M_C.

$$c_{strand} = \frac{\rho}{M_C} \tag{4.12}$$

The concentration of network strand should be related with the concentration of crosslinking agent.

$$c_{HX} = \frac{f_C \rho}{M_{HX}} \tag{4.13}$$

Here, f_C is functionality of crosslinking agent. In derivation of eq. 4.13, it was assumed that the extent of crosslinking reaction is 1. I did not check the actual extent of reaction, but it is noted that our reaction condition is widely used for molding of phenolic resins and known that the extent of reaction is close to 1. The two concentrations, c_{strand} and c_{HX} are compared in Figure 4.5.

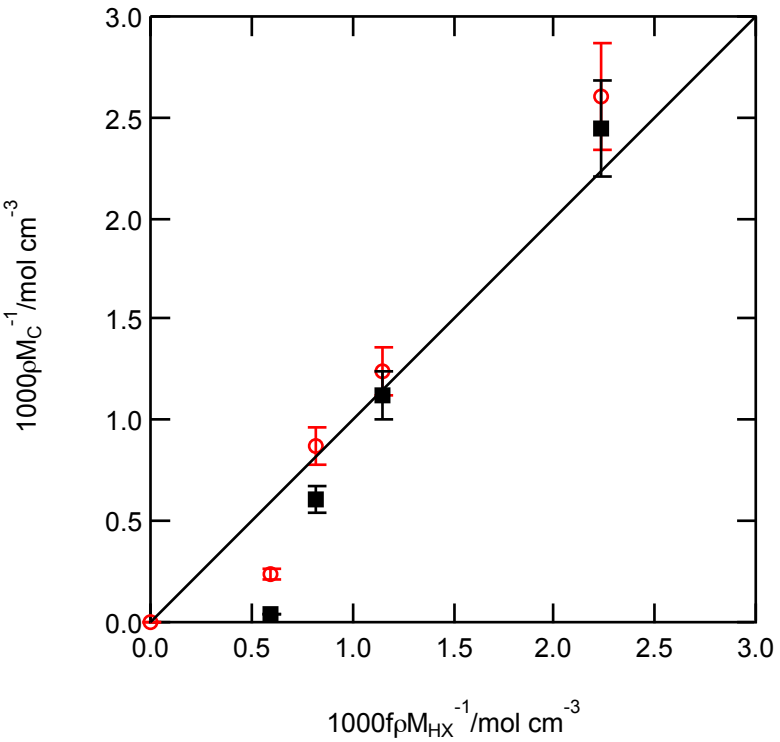

Figure 4.5 Comparison of concentration of network strand estimated from birefringence measurement and concentration of crosslinking agent (open circle). The closed squares represent after correction of contribution of the third hard core component.

Figure 4.5 clearly indicates that the two concentrations, c_{strand} and c_{HX} agree well with each other, except for Hx/NV-1.6 having the lowest crosslink agent. Thus, M_C obtained from birefringence relaxation is well correlated with the concentration of crosslinking agent. The data point for Hx/NV-1.6 deviates from the proportionality. This may be related to some other effects such as entanglements. Thus, we conclude that birefringence measurements are very effective to characterize the network structure.

4.4. Discussion.

Now, our question is why the rubbery plateau modulus, $E'(0)$, is insensitive to the crosslinking structure. The present analysis indicates that the ordinary stress-optical rule and the modified stress-optical rule composed of the two components do not hold well even for Hx/NV-1.6. The rubbery plateau modulus at high temperatures cannot be simply related with the orientation of network strand. The C_R value depending on crosslinking density also supports this conclusion.

Since two components version of MSOR did not work for phenolic resins, we consider the third component of stress. If the pre-polymer, novolac, has a small hard core due to its hyperbranched structure, the resulting network would contain the same hard core parts in it. In a previous study, we attribute the molecular origin of the glassy component to reorientational motion of structure unit of around the main chain axis. [15, 16] According to this interpretation, branched structure cannot rotate around the main chain axis. Thus, branching causes non-relaxation glassy component. If we consider such hard cores due to branching as the third component, the MSOR may be written as follows

$$E'(\omega)=(1-\phi_{HC})(E'_R(\omega)+E'_G(\omega))+\phi_{HC}\,E'_{HC} \tag{4.14}$$

$$O'(\omega)=(1-\phi_{HC})(C_R\,E'_R(\omega)+C_G\,E'_G(\omega))+\phi_{HC}\,C_{HC}\,E'_{HC} \tag{4.15}$$

Here, ϕ_{HC} is volume fraction of hard core parts and E'_{HC} is the constant modulus of the hard cores. In the following, we assume that the hard core part is the glassy and does not

relax with time even at higher temperatures than the glass transition temperature because of restriction of molecular motion brought by the very high crosslinking density. To discuss the validity of eqs. 4.14 and 4.15, we calculate the limiting values at high and low frequencies. If we further assume $E'_{HC} = E'_G(\infty)$ and $C_{HC} = C_G$, we obtain

$$E'(\infty) = (1-\phi_{HC})E'_R(\infty) + E'_G(\infty) \tag{4.16}$$

$$O'(\infty) = (1-\phi_{HC})(C_R\, E'_R(\infty)) + C_G\, E'_G(\infty) \tag{4.17}$$

Similarly, at low frequencies, we obtain

$$E'(0) = (1-\phi_{HC})(E'_R(0)) + \phi_{HC} E'_G(\infty) \tag{4.18}$$

$$O'(0) = (1-\phi_{HC}) C_R\, E'_R(0) + \phi_{HC} C_G\, E'_G(\infty) \tag{4.19}$$

Eqs. 4.18 and 4.19 explain why the phenolic resins show the higher plateau modulus and why the ordinary stress optical rule does not hold. For the modulus in the rubbery zone, significant contribution of HC component exists in addition to the R components. Since $E'(0) \sim 0.1$ GPa $\sim \phi_{HC} E'_G(\infty) > E'_R(0)$ and $E'_G(\infty) \sim 3$GPa, we estimate $\phi_{HC} = 0.03$.

In the previous section, we compare $O'(\infty) - C_G\, E'_G(\infty)$ and $O'(0)$ to evaluate M_C. According to eqs. 4.17 and 4.18, we should compare $O'(\infty) - C_G E'_G(\infty)$ and $O'(0) - \phi_{HC} C_G E'_G(\infty)$. Thus determined M_C is shown in Figure 4.5. The effect of subtraction of $\phi_{HC} C_G E'_G(\infty)$ is not so significant if crosslinking density is high.

In summary, we have firstly shown that the birefringence - stress relationship

for the phenolic resins cannot be described with the ordinary modified stress-optical rule, which works well for the most of ordinary amorphous polymers. The present analysis shows that the phenolic resins are not homogeneous and contain small amount (3 vol%) of non-relaxing hard core, which is probably produced in the pre-polymer due to the branching. The molecular motion of the structure units at the branching points would be highly restricted and therefore the units behave as non-relaxing elastic units. Such an inhomogeneous structure or two phase structure have been proposed.[17] Izumi *et al*. showed that linear strands of phenolic resins grow at beginning of gelation followed small structures form between strands by reaction of crosslinking with small angle X-ray Scattering experiments.[18] Such a scenario for crosslinking process does not contradict our present conclusion.

4.5. References

1. Baekeland, L. H. *USA Patent 942699*, **1907**.
2. Crespy, D.; Bozonmet, M.; M. Meier. *Angew. Chem. Int. Ed* **2008**, 47, 3322.
3. Gardziella, A.; Pilato, L. A.; Knop, A., *Phenolic Resins: Chemistry, Applications, Standardization, Safety and Ecology*. 2nd ed.; Springer: Berlin, **1999**.
4. Doi, M.; Edwards, S. F., *The Theory of Polymer Dynamics.* Clarendon: Oxford, **1986**; p 391.
5. Janeschitz-Kriegl, H., *Polymer Melt Rheology and Flow Birefringence.* Springer-Verlag: Berlin, **1983**; p 524.
6. Inoue, T.; Okamoto, H.; Osaki, K. *Macromolecules* **1991**, 24, 5670.

7. Iwawaki, H.; Inoue, T.; Nakamura, Y. *Macromolecules* **2011**, 44, 5414.
8. Iwawaki, H.; Urakawa, O.; Inoue, T.; Nakamura, Y. *Macromolecules* **2012**, 45, 4801.
9. Maji, S.; Urakawa, O.; Inoue, T. submitted.
10. Hwang, E. J.; Inoue, T.; Osaki, K. *Polymer* **1993**, 34, 1661.
11. Ferry, J. D., Chapter 11 Dependence of Viscoelastic Behavior on Temperature and Pressure. In *Viscoelastic Properties of Polymers*, 4th Ed. ed.; Wiley: New York, **1980**; pp 264.
12. Treloar, L. R. G., T*he Physics of Rubber Elasticity*. Clarendon: Oxford, **1958**.
13. Inoue, T.; Osaki, K. *Macromolecules* **1996**, 29, 1595.
14. Kuhn, W.; Grun, F. *Kolloid Z.* **1942**, 101, 248.
15. Inoue, T.; Matsui, H.; Murakami, S.; Kojiya, S.; Osaki, K. *Polymer* **1997**, 38, 1215.
16. Inoue, T.; Matsui, H.; Osaki, K. *Rheol. Acta* **1997**, 36, 239.
17. Misra, S. C.; Manson, J. A.; Sperling, L. H. *ACS Symposium* **1979**, 114, 157.
18. Izumi, A.; Nakao, T.; Shibayama, M. *Soft matter* **2013**, 9, 4188.

Chapter 5 Summary

In this thesis, the relationship of structure and rheological property of highly cross-linked polymers were investigated by using small angle X-ray scattering, viscoelastic relaxation, and spectroscopy measurements. The hierarchical structures by hydrogen bond were estimated by SAXS. The cross linking and branching structures of phenolic resins were estimated by NMR and rheo-optical measurement.

In chapter 2, dynamic viscoelasticity of three novolac resins having different molar mass and different methylene linkage pattern content, para-para', ortho-ortho', and ortho-para' methylene linkages, were examined to clarify the relationship between structure and viscoelastic properties of novolac resins. Content of linkage pattern of the novolacs was evaluated by ^{13}C NMR measurements. GPC measurements elucidated that number density distribution function was close to that predicted for the hyperbranched chains. Molar mass dependence of the intrinsic viscosity indicated that the three novolacs had a compact branched chain structure similarly to the hyperbranched chains. The glass transition temperature determined by DSC depended on molar mass and less sensitive to methylene linkage pattern. Viscoelastic spectra obtained by the method of reduced variables for the three resins were similar to each other because the glassy relaxation was dominant. Weak polymeric modes originated by the chain connectivity were observed at low frequencies of the composite curve and were well described with the dynamic scaling theory for the hyperbranched chains. And we estimated the

segment size, M_S, of novolac is M_S=350 by rheo-optical analysis. The effect of linkage pattern on mechanical properties was not clearly observed.

In chapter 3, relationship of hierarchical structure and rheological properties of H-bonding system, poly (vinyl acetate -co- vinyl alcohol)s, were discussed. The aggregation structures revealed by small angle X-ray scattering were characterized by the Debye-Bueche type scattering profiles with the characteristic lengths of 1~3nm for the samples with the vinyl alcohol content higher than 35%. In contrast no characteristic scattering for lower OH samples was observed. Linear viscoelastic data were analyzed based on the mean filed type random branching model. For the samples with the OH content lower than 28%, the theory was found to give good predictions for the viscoelastic spectra. In contrast deviations from the theory appeared for the OH contents higher than 35%. To explain the discrepancy, the effects of the emergence of entanglement and the extra relaxation due to the dissociation of H-bonding aggregates were added to the theoretical equation. I obtained fairly well fitting results and concluded that the multiple H-bonding systems were in the vulcanization universal class.

In chapter 4, relationship of cross-linking structure and rheological property of phenolic resins were quantitatively analyzed. Dynamic viscoelasticity and dynamic birefringence of phenolic resins having different cross-linking density were examined to clarify the relationship between structure and viscoelastic properties. Dynamic modulus were found to be insensitive to crosslinking density at high crosslinking density where molar mass between the crosslinking points was smaller than the viscoelastic segment

size of phenolic resin while the complex strain-optical coefficient reflects more sensitively the crosslinking density. And we estimated the molar mass of network strand between crosslinking points, M_C, of phenolic resins, M_C=5900, 1200, 900 and 520 for Hx/NV-1.6, Hx/NV-2.2, Hx/NV-3.1 and Hx/NV-6.0, respectively. These results provide a universal method to characterize highly crosslinking polymers, in particular viscoelastic properties of branched polymers. Fundamental understanding of crosslinking and highly branching materials is quite important for future studies concerning more complex systems.

Publications List

1. Satoshi Maji, Osamu Urakawa and Tadashi Inoue. "Structure and Viscoelasticity of Novolac Resins", submitted to *Polymer Journal*. (**Chapter 2**)
2. Satoshi Maji, Miho Fujita, Osamu Urakawa and Tadashi Inoue. "Structural Analysis of Poly (vinyl acetate -co- vinyl alcohol) by Small and Wide Angle X-ray Scattering", submitted to *Polymer*. (**Chapter 3**)
3. Satoshi Maji, Osamu Urakawa and Tadashi Inoue (2014). "Viscoelastic Properties and Birefringence of Phenolic Resins", *Polymer Journal*. in press. DOI: 10.1038/pj.2013.97. (**Chapter 4**)

Other Works

1. Kotera, M., B. Samyul, K. Araie, Y. Sugioka, T. Nishino, S. Maji, M. Noda, K. Senoo, T. Koganezawa and I. Hirosawa (2013). "Microstructures of BPDA-PPD polyimide thin films with different thicknesses." *Polymer* **54**(9): 2435-2439. DOI: 10.1016/j.polymer.2013.03.005
2. Maji, S. (2013). "Dielectric Property measurement in High Frequency Range for Network Polymers." *Journal of Network Polymer, Japan* **34**(6): 336-342. DOI: 10.11364/networkpolymer.34.336
3. Maji, S. and T. Izumikawa (2008). "Measurement Technique of Dielectric Anisotropy of Polymers at GHz Bands." *Journal of Network Polymer, Japan* **29**(2): 101-105. DOI: 10.11364/networkpolymer1996.29.101
4. Maji, S., O. Urakawa and K. Adachi (2007). "Relationship between segmental dynamics and tracer diffusion of low mass compounds in polyacrylates." *Polymer* **48**(5): 1343-1351. DOI: 10.1016/j.polymer.2006.12.039